

# Cosmic UHE Neutrino Signatures

K. Giesel, J.-H. Jureit, E. Reya

*Universität Dortmund, Institut für Physik,  
D-44221 Dortmund, Germany*

## Abstract

Utilizing the unique and reliable ultrasmall- $x$  predictions of the dynamical (radiative) parton model, nominal event rates and their detailed energy dependence caused by a variety of cosmic UHE neutrino fluxes are calculated and analyzed. In addition, maximal Regge-model inspired small- $x$  structure functions are employed for obtaining optimal rates which do not necessarily require ‘new’ physics interpretations. Upward  $\mu^+ + \mu^-$  event rates are estimated by taking into account total and nadir-angle dependent regeneration effects due to neutral current interactions. For exploring extragalactic neutrino sources at highest energies ( $\gtrsim 10^8$  GeV) with modern (future) ground-level telescopes, we analyze horizontal air shower event rates and shower events caused by Earth-skimming tau-neutrinos, in particular their detailed shower- and cosmic neutrino-energy dependence. As an illustration of ‘new physics’ implications we estimate the relevant horizontal air shower event rates due to spin-2 Kaluza-Klein ‘graviton’ exchanges in neutral current neutrino-quark and neutrino-gluon interactions at low TeV-scales.

# 1 Introduction

Detection of cosmic ultrahigh-energy (UHE) neutrinos with energies above  $10^{16}$  eV is one of the important challenges of cosmic ray detectors in order to probe the faintest regions of the Universe that are otherwise shielded from us by large amounts of matter. Their observation will probe particle (possibly ‘new’) physics as well as astrophysics phenomena such as galaxy formation. The sources of UHE neutrinos range, however, from the well established to the highly speculative [1, 2, 3, 4, 5]. The well measured cosmic rays up to the GZK cutoff [6] at around  $5 \times 10^{19}$  eV, where they necessarily interact with the 2.7 K cosmic microwave background through  $p\gamma \rightarrow n\pi^+$ , produce the ‘guaranteed’ (cosmogenic) flux of ‘Greisen neutrinos’ when the pions decay [6, 7]. In addition, far larger neutrino fluxes are predicted in models of active galactic nuclei (AGN) [8, 9, 10], gamma ray bursts (GRB) [11], decays of exotic heavy particles of generic top-down or topological defects (TD) [12, 13, 14, 15, 16] and  $Z$ -bursts [17, 18]. Representative fluxes of some hypothesized sources are displayed in Fig. 1 which we shall use for all our subsequent calculations. For illustration the steeply falling background atmospheric (ATM) neutrino flux [19, 20, 21] is shown as well which originates from (anti)neutrinos produced by cosmic ray interactions in the Earth’s atmosphere.

Besides these violently different model expectations for (anti)neutrino fluxes, there are further uncertainties when calculating event rates for neutrino telescopes due to the sensitivity of  $\nu N$  cross sections to the parton distributions in the yet unmeasured ultrasmall Bjorken- $x$  region,  $x < 10^{-5}$ , not accessible at the weak scale  $M_W$  by deep inelastic scattering (DIS) experiments. At the highest (anti)neutrino energies  $E_\nu$  shown in Fig. 1, contributions from the region around  $x \simeq M_W^2/2M_N E_\nu \simeq 10^{-8}$  to  $10^{-9}$  become non-negligible and therefore known structure functions and parton distributions at  $x \gtrsim 10^{-5}$  have to be extrapolated to  $x < 10^{-5}$  as soon as  $E_\nu \gtrsim 10^8$  GeV. (Here one commonly assumes that the DIS small- $x$  measurements at  $x \gtrsim 10^{-5}$  and moderate momentum scales  $Q^2$  can be safely

evolved to the relevant scale  $Q^2 = M_W^2$  by standard QCD renormalization group (RG) techniques.) Such extensive extrapolations are performed either of fits to existing data at  $x \gtrsim 10^{-5}$  using specific, possibly arbitrary and unreliable, assumptions (e.g. various fixed power behaviors in  $x$  of structure functions as  $x \rightarrow 0$ ) [20, 21, 22, 23, 24, 25, 26] or by using [27, 28] the QCD inspired dynamical (radiative) parton model which proved to provide reliable high energy predictions [29, 30, 31, 32] in the past [33, 34]. Within this latter approach the entire partonic (gluons and (anti)quarks) structure at small fractional momenta  $x \lesssim 10^{-2}$  can be understood and calculated via RG evolutions from first principles, i.e. QCD dynamics, independently of any free (fit) parameter in the small- $x$  region due to valence-like gluon and sea input densities at some low momentum scale  $Q_0 \simeq 0.5 - 0.6$  GeV [30, 31, 32]. Having successfully predicted the small- $x$  behavior of structure functions between  $x = 10^{-2}$  to  $10^{-5}$  prior to experiments, it is not unreasonable to expect the unambiguous dynamical results of the radiative parton model between  $x = 10^{-5}$  and  $10^{-8}$  or  $10^{-9}$  to be reliable as well. These ultrasmall- $x$  predictions are furthermore perturbatively stable and unique at the relevant momentum scales  $Q^2 \simeq M_W^2$  [32]. Moreover, consistent BFKL model resummations of subleading  $\ln \frac{1}{x}$  contributions in leading order QCD yield remarkably similar results [35] even at highest neutrino energies of  $10^{12}$  GeV.

A detailed analysis [36] has shown that within the radiative parton model all relevant (anti)neutrino-nucleon cross sections can be calculated with an uncertainty of typically about  $\pm 20\%$  at highest neutrino energies of  $10^{12}$  GeV. We shall adopt this approach for all our subsequent calculations, in particular the canonical GRV98 parton distributions [32] in next-to-leading order QCD will serve as our appropriate nominal benchmark set of densities. Notice that cross sections obtained from the fitted CTEQ3-DIS parametrizations [37] at  $x \gtrsim 10^{-5}$  with their assumed fixed-power extrapolation to  $x < 10^{-5}$ , as used in [20], accidentally coincide practically with the ones derived from the ultrasmall- $x$  dynamical predictions of the radiative parton model [36]; only at highest neutrino energies of  $10^{12}$  GeV, i.e.  $x \simeq 10^{-8}$  to  $10^{-9}$ , they are about 10% larger than the radiatively generated ones.

Actual calculations of event rates could therefore also be performed with the CTEQ3–DIS densities which are easier to use since heavy quarks ( $c$ ,  $b$ ,  $t$ ) are effectively (but less adequately) treated as massless intrinsic partons, in contrast to the more appropriate but also more cumbersome explicit calculation of massive heavy quark contributions required when using the ‘fixed flavor’ GRV98 densities [32]. (A comparison of the two approaches can be found in [36].) Similar remarks hold true for the CTEQ4–DIS parametrizations [38], used in [21], which underestimate, relatively to GRV98, the neutrino cross sections by about 20% at  $E_\nu \simeq 10^{10} - 10^{12}$  GeV.

The detection of UHE cosmic neutrinos is, however, extremely difficult. For energies below  $10^8$  GeV it is widely believed that one of the most appropriate techniques for neutrino detection consists of detecting the Čerenkov light from muons or showers produced by CC and NC neutrino interactions of mainly upward–going neutrinos in large–volume underground water or ice detectors such as AMANDA/IceCube, NESTOR and ANTARES [2, 39]. However, above 40 TeV the Earth’s diameter exceeds the interaction length of neutrinos and their shadowing in the Earth rapidly increases above 100 TeV [20, 21] which severely restricts rates in underground detectors which are bounded by detection volumes of at most  $1 \text{ km}^3$ . Eventually it becomes beneficial to look for events induced by downward–going and (quasi)horizontal neutrinos, provided of course that downward–going events produced by interactions within the instrumented underground detector volume can be efficiently observed. At energies above  $10^8$  GeV, where the (anti)neutrino interaction length is below about  $10^3$  km water equivalent in rock, upward–going neutrinos are blocked by Earth and thus under–water and under–ice km–scale detectors become ineffective due to the opaqueness of Earth to upward neutrinos. Therefore large–area ground arrays or surface fluorescence telescopes such as AGASA, the HiRes detector, the Pierre Auger Observatory and the Telescope Array [26, 28, 40, 41], for which the interaction medium is not the Earth but the atmosphere, could become instrumental in exploring the whole spectrum of cosmic neutrino fluxes up to highest

neutrino energies of about  $10^{21}$  eV shown in Fig. 1. In particular, a novel alternative method for detecting UHE (anti)neutrinos with  $E_\nu > 10^8$  GeV has been recently suggested via Earth-skimming neutrinos [42, 43, 25], dominantly  $\nu_\tau$  travelling at large nadir angles producing ‘double bang’ events in the atmosphere when converting to tau-leptons exiting the Earth’s surface which, when decaying, produce the second shower bang.

When upward-going UHE neutrinos penetrate through the Earth, they undergo attenuation (absorption) due to charged and neutral current interactions as well as regeneration [44, 45] due to the neutral current interactions (which shift their energy rather than absorbing them) at high energies. The NC shifts the neutrino energies to lower energies and, in addition, regeneration populates the lower energy part of the flux spectra shown in Fig. 1. In Sect. 2 we shall perform detailed calculations of these regeneration effects [35] not only for our representative fluxes in Fig. 1 but in particular also for the expected event rates for modern underground detectors. Depending on the shape of the neutrino flux, these effects can be substantial, i.e. increase the non-regenerated event rates on the average by about 20%. For comparison we therefore have also to recalculate, for our representative fluxes in Fig. 1, the upgoing event rates where regeneration effects have not been taken into account when calculating the shadow factor [20, 21, 23]. In addition we show in detail what high-energy bins of the original fluxes in Fig. 1 remain experimentally accessible after their depletion and regeneration due to NC interactions at highest neutrino energies. Furthermore, downward events initiated by UHE neutrinos will be also calculated using recent Regge-inspired power-like small- $x$  extrapolations in order to learn about possible upper bounds of event rates which may be accommodated by ‘conventional’ standard model approaches and which do not necessarily require ‘new’ physics interpretations. Along similar lines we study in Sect. 3 event rates of quasi-horizontal air showers to be detected by large area ground arrays and surface air fluorescence telescopes, as well as of Earth-skimming UHE  $\nu_\tau$ ’s which will allow to test cosmic neutrino flux models at highest energies,  $E_\nu \gtrsim 10^8$  GeV. We shall in particular be interested to what extent

shower rates as measured in certain bins of  $E_{\text{sh}}$  or  $E_{\tau}$  will be able to explore and delineate specific features of the energy profile of the various predicted incoming cosmic neutrino fluxes  $\Phi(E_{\nu})$  in Fig. 1. Finally, as an illustration of possible implications of ‘new’ physics, we present in Sect. 4 highly speculative expectations of string theories with large ‘extra dimensions’ for the relevant quasi–horizontal air shower event rates. Section 5 summarizes our results.

## 2 Event Rates for Underground Čerenkov–Detectors

The upward-muon event rate depends on the  $(\nu_{\mu})N$  cross section through the interaction length  $\lambda_{\text{int}}$  that governs the attenuation of the original neutrino flux due to interactions in the Earth as described by the shadow factor  $S$  as well as through the probability  $P_{\mu}$  that the neutrino converts to a muon energetic enough to arrive at the detector with energy  $E_{\mu}$  larger than the assumed threshold energy  $E_{\mu}^{\text{min}}$ . The total (nadir angle integrated) upward–muon event rate per second in a detector with an energy dependent area  $A(E_{\mu})$  is then given by [20, 21]

$$\text{rate} = 2\pi \int_{E_{\mu}^{\text{min}}} dE_{\nu} \int_0^{1-E_{\mu}^{\text{min}}/E_{\nu}} dy A(E_{\mu}) P_{\mu}(E_{\nu}, y; E_{\mu}^{\text{min}}) S(E_{\nu}) \frac{d\Phi_{\nu}}{dE_{\nu}} \quad (2.1)$$

where the factor of  $2\pi$  is the effective solid angle for upward muons,  $E_{\mu} = (1 - y)E_{\nu}$  and  $\Phi_{\nu}(E_{\nu})$  refers to the original cosmic neutrino fluxes shown in Fig. 1 incident on the surface of the Earth (i.e.  $\Phi_{\nu, \bar{\nu}} = \Phi/4$ ) before they undergo attenuation and regeneration. Unless otherwise stated, the energy integration is always extended to the highest energy of  $10^{12}$  GeV in Fig. 1. Furthermore,

$$P_{\mu}(E_{\nu}, y; E_{\mu}^{\text{min}}) = N_A R(E_{\mu}, E_{\mu}^{\text{min}}) \frac{d\sigma_{CC}^{\nu N}(E_{\nu}, y)}{dy} \quad (2.2)$$

with  $N_A = 6.022 \times 10^{23} g^{-1}$  and where all relevant expressions for calculating CC and NC  $(\nu)N$  cross sections in the ‘fixed flavor’ and ‘variable flavor’ scheme can be found in [36].

It may be helpful to notice that, for an energy-independent effective detector area  $A_{\text{eff}}$ , (2.1) reduces to the more common expression [20, 21]

$$\text{rate} = 2\pi A_{\text{eff}} \int_{E_{\mu}^{\text{min}}} dE_{\nu} P_{\mu}(E_{\nu}; E_{\mu}^{\text{min}}) S(E_{\nu}) \frac{d\Phi_{\nu}}{dE_{\nu}} \quad (2.3)$$

with

$$P_{\mu}(E_{\nu}; E_{\mu}^{\text{min}}) = N_A \sigma_{CC}^{\nu N}(E_{\nu}) \langle R(E_{\nu}; E_{\mu}^{\text{min}}) \rangle \quad (2.4)$$

and the average range  $\langle R \rangle$  of a muon in rock is given by [20]

$$\langle R(E_{\nu}; E_{\mu}^{\text{min}}) \rangle = \frac{1}{\sigma_{CC}^{\nu N}(E_{\nu})} \int_0^{1-E_{\mu}^{\text{min}}/E_{\nu}} dy R((1-y)E_{\nu}, E_{\mu}^{\text{min}}) \frac{d\sigma_{CC}^{\nu N}(E_{\nu}, y)}{dy}. \quad (2.5)$$

The range  $R$  of an energetic muon in (2.2) and (2.5) follows from the energy-loss relation [46]

$$-dE_{\mu}/dX = \alpha_{\mu}(E_{\mu}) + \beta_{\mu}(E_{\mu}) E_{\mu} \quad (2.6)$$

with  $X$  being the thickness of matter traversed by the muon in units of  $g/\text{cm}^2 = \text{cm we}$ . Despite the very weak energy dependence [46] of the ionization loss  $\alpha_{\mu}(E_{\mu})$  we use [20, 46]  $\alpha_{\mu} = 2.0 \times 10^{-3} \text{ GeV (cm we)}^{-1}$  since the effect of  $\alpha_{\mu}$  is negligible for high energies. Assuming the fractional energy loss  $\beta_{\mu}(E_{\mu})$  to be energy independent as well, for example [20, 21, 46]  $\beta_{\mu} = 3.9 \times 10^{-6} \text{ (cm we)}^{-1}$  or [25, 46]  $\beta_{\mu} = 6.0 \times 10^{-6} \text{ (cm we)}^{-1}$ , the relation (2.6) can be integrated analytically,

$$R(E_{\mu}, E_{\mu}^{\text{min}}) \equiv X(E_{\mu}^{\text{min}}) - X(E_{\mu}) = \frac{1}{\beta_{\mu}} \ln \frac{\alpha_{\mu} + \beta_{\mu} E_{\mu}}{\alpha_{\mu} + \beta_{\mu} E_{\mu}^{\text{min}}}. \quad (2.7)$$

Alternatively, using a QED-oriented energy dependence [47]

$$\begin{aligned} \alpha_{\mu}(E_{\mu}) &= [2.033 + 0.077 \ln(E_{\mu}/\text{GeV})] \times 10^{-3} \text{ GeV (cm we)}^{-1} \\ \beta_{\mu}(E_{\mu}) &= [2.229 + 0.2 \ln(E_{\mu}/\text{GeV})] \times 10^{-6} \text{ (cm we)}^{-1}, \end{aligned} \quad (2.8)$$

(2.6) has to be integrated numerically. In Fig. 2 we show the average muon ranges resulting from these three different choices and compare them with the Monte Carlo result of Lipari and Stanev [48] where regeneration has been taken into account and which has

been presented only up to  $10^9$  GeV. Since this latter Monte Carlo result agrees best with our result using a constant  $\alpha_\mu$  and  $\beta_\mu = 6.0 \times 10^{-6} \text{ (cm we)}^{-1}$ , this choice appears to be best suited for extrapolations beyond  $10^9$  GeV and we therefore will utilize it for our subsequent calculations. Needless to say that this conclusion is independent of the specific choice of parton distributions since obviously  $\langle R \rangle$  in (2.5) does practically not depend on them. (If instead the numerical range of Fig. 2 were used, the resulting event rates would be about 30% larger.)

Next we turn to the shadow factor in (2.1) describing the attenuation (due to  $\sigma_{\text{tot}} = \sigma_{CC} + \sigma_{NC}$ ) and regeneration (due to  $\sigma_{NC}$ ) of (anti)neutrinos when penetrating through the Earth. Both effects are summarized in the transport equation [44, 45] for the neutrino flux  $\Phi_\nu(E, X)$  at ‘depth’  $X$

$$\frac{d\Phi_\nu(E_\nu, X)}{dX} = -\frac{1}{\lambda_{\text{int}}(E_\nu)} \Phi_\nu(E_\nu, X) + N_A \int_0^1 \frac{dy}{1-y} \frac{d\sigma_{NC}^{\nu N}(E_y, y)}{dy} \Phi_\nu(E_y, X) \quad (2.9)$$

where the neutrino interaction length is defined by  $\lambda_{\text{int}} = 1/(N_A \sigma_{\text{tot}}^{\nu N})$ , the fractional energy loss by  $E_y = E_\nu/(1-y)$  and  $\Phi_\nu(E_\nu, 0) = \Phi_\nu$  where  $\Phi_\nu = \Phi_\nu(E_\nu)$  is related to the initial unmodified fluxes as shown in Fig. 1. It turns out to be convenient to solve this equation iteratively via the ansatz [35]

$$\Phi_\nu(E_\nu, X)/\Phi_\nu(E_\nu) = \exp[-N_A \sigma_{\text{tot}}^{\nu N}(E_\nu)X] \Psi_\nu(E_\nu, X), \quad (2.10)$$

i.e.,

$$\begin{aligned} \frac{d\Psi_\nu(E_\nu, X)}{dX} &= N_A \int_0^1 \frac{dy}{1-y} \frac{\Phi_\nu(E_y)}{\Phi_\nu(E_\nu)} \\ &\exp\{-N_A [\sigma_{\text{tot}}^{\nu N}(E_y) - \sigma_{\text{tot}}^{\nu N}(E_\nu)]X\} \frac{d\sigma_{NC}^{\nu N}(E_y, y)}{dy} \Psi_\nu(E_y, X). \end{aligned} \quad (2.11)$$

(It should be noticed that this solution can be found even more efficiently by using [45], instead of the r.h.s. of (2.10),  $\exp[-X/\Lambda_\nu(E_\nu, X)]$  with an effective absorption length  $\Lambda_\nu(E_\nu, X) \equiv \lambda_{\text{int}}/[1 - Z_\nu(E_\nu, X)]$ .) According to (2.10), the total shadow factor is given by

$$S(E_\nu) = \frac{1}{2\pi} \int_0^{2\pi} d\varphi \int_0^{\pi/2} d\theta \sin \theta \exp[-N_A \sigma_{\text{tot}}^{\nu N}(E_\nu)X(\theta)] \Psi_\nu(E_\nu, X(\theta)) \quad (2.12)$$



where the  $d\varphi$  integration is trivial for our isotropic (anti)neutrino fluxes. The amount of material encountered by an upward-going neutrino in its passage through the Earth is given by the column depth  $X(\theta)$  which depends upon the nadir angle  $\theta$  between the normal to the Earth's surface (passing through the detector) and the direction of the neutrino beam incident on the detector ( $\theta = 0^\circ$  corresponds to a beam traversing the diameter of the Earth). It is obtained from integrating the density  $\rho(r)$  of Earth [49] along the neutrino beam path at a given  $\theta$  and is given in Fig. 15 of [20] where  $X(\theta)$  has been denoted by  $z(\theta)$ . For definiteness all above formulae have been given for an incoming neutrino beam, but similar expressions hold of course for antineutrinos.

Before evaluating total event rates, we first compare the effects of attenuation and regeneration in (2.10) for the initial differential  $\nu + \bar{\nu}$  fluxes in Fig. 1 when they reach the Earth's surface ( $\Phi_{\nu,\bar{\nu}}(E_\nu) = \Phi(E_\nu)/4$ ), with the pure attenuation (absorption) where regeneration is omitted ( $\Psi_{\nu,\bar{\nu}} \equiv 1$  in (2.10)). Some typical representative results for the differential shadow factor in (2.10) are shown in Fig. 3 where, for comparison, the pure attenuation (absorption) is shown by the dashed curves. The results for  $\nu$  and  $\bar{\nu}$  fluxes are shown separately in Fig. 3(a) and Fig. 3(b), respectively, which are combined in Fig. 3(c) for the total fluxes in Fig. 1. For the rather flat (initial) cosmic fluxes in Fig. 1, the regeneration effect is significant and increases the fluxes at the detector by as much as 30% for  $\theta = 0^\circ$  and about 10% for  $\theta = 40^\circ$  as compared to the purely absorbed (attenuated) fluxes. In fact it can even enhance the initial flux at lower energies ( $E_\nu \lesssim 10^4$  GeV) at  $\theta \lesssim 40^\circ$  as shown for the AGN-SS flux in Fig. 3. A similar result was originally found in [44] investigated in more detail in [35] for (even somewhat flatter) actual neutrino fluxes. Below  $10^6$  GeV the shadow factors for antineutrinos in Fig. 3(b) are obviously larger than the ones for neutrinos in Fig. 3(a), since  $\sigma^{\bar{\nu}N} < \sigma^{\nu N}$ , except for the regenerated AGN-SS flux at  $\theta = 0^\circ$  below  $10^4$  GeV where, in addition, AGN-SS strongly decreases for decreasing  $E_\nu$  as can be seen in Fig. 1. At larger energies ( $E_\nu \gtrsim 10^6$  GeV), where the CC and NC cross sections for neutrinos and antineutrinos practically coincide, the

shadow factors in Figs. 3(a) and 3(b) become indistinguishable. Clearly, once the energy is sufficiently high the attenuation factor  $\exp(-N_A \sigma_{\text{tot}}^{(-)\nu} X)$  leads to total shadowing as seen in Fig. 3 due to the increase of (anti)neutrino cross sections with energy. The smaller the nadir angle the lower the energy of complete attenuation.

For experimental purposes the relevant and interesting quantity is the total  $\nu + \bar{\nu}$  flux  $\Phi_{\nu+\bar{\nu}}(E_\nu, X)$  reaching the detector, after its passage through Earth, at different nadir angles  $\theta$ . The four plots in Figs. 4(a) and 4(b) show first the initial  $\nu + \bar{\nu}$  fluxes reaching the Earth's surface,  $\Phi_{\nu+\bar{\nu}}(E_\nu, X = 0) \equiv \Phi_{\nu+\bar{\nu}}(E_\nu) = \Phi(E_\nu)/2$  with the original cosmic fluxes  $\Phi$  being given in Fig. 1, and then the fluxes at the detector  $\Phi_{\nu+\bar{\nu}}(E_\nu, X)$  for the three nadir angles  $\theta = 80^\circ$ ,  $40^\circ$  and  $0^\circ$ . (Recall that  $0^\circ$  is the passage of (anti)neutrinos through the center of the Earth.) Due to the large  $^{(-)\nu}N$  cross sections the attenuation effects (absorption plus regeneration) reduce dramatically the fluxes of ultrahigh energy (anti)neutrinos, particularly at small nadir angles in Fig. 4. For convenience of reference the atmospheric (ATM) neutrino flux is shown in both Figs. 4(a) and 4(b). The AGN fluxes in Fig. 4(a) stand out above this background ATM neutrino spectrum for neutrino energies above about  $10^5$  GeV, whereas the flatter TD and  $Z$ -burst fluxes in Fig. 4(b) are overwhelmed by the ATM background below  $10^6$  GeV, in particular for smaller nadir angles. Nevertheless there remains a window for the observation of cosmic neutrinos (with  $E_\nu \lesssim 10^8$  GeV) by underground detection of the energetic  $\mu^\pm$  when calculating total event rates.

The total upward  $\mu^+ + \mu^-$  event rates are calculated according to (2.1) for the (forthcoming) AMANDA-II [2, 50], IceCube [51] and ANTARES [39] detectors with their respective energy dependent areas  $A(E_\mu)$  shown in Fig. 5. The required total  $\nu_\mu$  and  $\bar{\nu}_\mu$  flux in (2.1) reaching the Earth's surface is given by  $\Phi_{\nu_\mu+\bar{\nu}_\mu} \equiv \Phi_{\nu_\mu} + \Phi_{\bar{\nu}_\mu} = \Phi/2$ , with the original cosmic neutrino fluxes  $\Phi$  given in Fig. 1, since the recent discovery of near-maximal  $\nu_e - \nu_\mu$  and  $\nu_\mu - \nu_\tau$  mixing [52] implies that the originally produced cosmic neutrino fluxes, having a  $\nu_e : \nu_\mu : \nu_\tau$  ratio of  $1 : 2 : 0$  at some astrophysical source, inevitably

oscillate [53, 54] to a ratio of 1 : 1 : 1. The resulting annual total nadir–angle–integrated rates are given in Table 1 where the numbers in parentheses are the event rates with no regeneration ( $\Psi \equiv 1$  in (2.10)), i.e. the attenuation of the Earth’s penetrating neutrinos is just due to naive absorption. Regeneration effects increase the event rates on the average by about 20% as compared to the ones where the attenuation of neutrinos is just caused by absorption [20, 21, 23]. The contribution to the event rates in Table 1 from energies above  $10^8$  GeV becomes, however, negligible and unmeasurably small due to the reduction of the initial neutrino fluxes by attenuation with or without regeneration. The highest signal rates arise in the AGN models which might be testable for neutrino flux energies as large as  $10^7 - 10^8$  GeV, i.e.  $E_\mu^{\min} = 10^7$  GeV. Beyond neutrino energies of  $10^8$  GeV, however, present models of cosmic neutrino fluxes are not testable by upward–going  $\mu^+ + \mu^-$  events. Notice that the atmospheric neutrino background becomes marginal for neutrino energies above  $10^5$  GeV [20, 21, 35], i.e.  $E_\mu^{\min} = 10^5$  GeV in Table 1, or in other words the ATM rate comes entirely from  $E_\nu < 10^6$  GeV. Furthermore the energy dependence of the upward–going muon rate in Table 1 will be an important discriminant for separating atmospheric and extraterrestrial sources. The nadir angular dependence of the annual upward  $\mu^+ + \mu^-$  event rates shown in Fig. 6 for two representative cosmic neutrino flux models illustrates in more detail the enhancement of event rates caused by regeneration. Apart from the absolute normalizations, these angular distributions are not too sensitive to the chosen value of  $E_\mu^{\min}$  and clearly favor shallow nadir angles, i.e. large  $\theta$ , where the largest amount of events reside. The dashed histograms in Fig. 6 refer to events where the neutrino attenuation is caused just by absorption ( $\Psi \equiv 1$  in (2.12)) with regeneration effects disregarded which give rise to the total event rates in parentheses in Table 1. Due to maximal  $\nu_\mu - \nu_\tau$  mixing, the  $\nu_\tau + \bar{\nu}_\tau$  flux arriving at the Earth’s surface may enhance these upward  $\mu^+ + \mu^-$  rates due to their interaction in Earth via  $\nu_\tau N \rightarrow \tau X \rightarrow \mu X'$  [55, 56, 57]. Here we disregard such additional contributions since Earth–skimming tau–neutrinos [42, 43, 25] will dominate over these interactions and allow to test cosmic neutrino flux models at highest energies to which we shall turn later.

The upward event rates studied thus far depend obviously rather little [20] on the specific choice of parton distributions since the combination  $P_\mu S$  in (2.3) is rather insensitive with respect to different choices: for increasing energies the effect of larger cross sections is to increase the probability  $P_\mu$  that a neutrino produces an observable muon, but also to increase the attenuation of neutrinos via  $S$  on their way to the detector. This is of course in contrast to the downward event rates for  $(\bar{\nu})$ 's that enter the detector from above or quasi-horizontally, i.e. where [20]  $S \simeq 1$ . For very high muon-energy thresholds it will thus be necessary to observe downward-going muons produced by interactions within the instrumented volume. Our expected annual downward  $\mu^+ + \mu^-$  event rates are shown in Table 2 which are of course consistent with the ones observed in [21] for appropriate fluxes and parameters used there. These results are encouraging and allow to test cosmic neutrino fluxes at higher neutrino energies (by about a factor of 10 higher than for the upward rates in Table 1), provided that downward-going contained events can be observed efficiently. For comparison we show again in Table 2 the background atmospheric ATM rates which, for the sizeable and measurable cosmic rates, play no role for  $E_\nu \gtrsim 10^6$  GeV. Despite the fact that underground muon detectors (will) have a poor energy resolution, a measurement of the energy dependence of the downward-going muon rate will be again an important discriminant for separating atmospheric and extraterrestrial sources below  $10^6$  GeV. (Notice that the downward muon rates in Tables 2 and 3 remain essentially unchanged if the detector depth is taken into account. Since underground detectors are deployed at a depth of 2 to 3 km, the limited amount of matter above the detector does not reduce the shadow factor  $S(E_\nu) \simeq 1$  in (2.3) which holds for all relevant energies in Tables 2 and 3. Only at energies as high as  $E_\nu = 10^{10}$  GeV it decreases to  $S = 0.99$ .)

Here the question arises whether some other reasonably founded extrapolation to the ultrasmall- $x$  region could sizeably enhance our benchmark rates (e.g. in Table 2) calculated from cross sections as derived from our nominal QCD-dynamical GRV98 parton distributions (or equivalently from the appropriately extrapolated CTEQ3-DIS parametriza-

tion). In particular for ‘new physics’ searches [1, 3, 4, 5, 13, 58, 59, 60] it will be important to know to what extent the conventional standard model would allow for (sizeably) larger rates. For this purpose we employ a Regge model inspired small- $x$  description of the DIS ep structure function  $F_2^{ep}(x, Q^2)$  recently suggested by Donnachie and Landshoff (DL) [61]. According to DL,  $F_2^{ep}$  may be written as a sum of three factorized terms  $f_i(Q^2)x^{-\varepsilon_i}$  to be fitted to DIS HERA data as well as to total photoproduction ( $Q^2 = 0$ ) cross sections. This result may be used as a (possibly extreme) guideline for an extrapolation into the ultrasmall- $x$  region, dominated by the ‘hard pomeron’ component  $\varepsilon_0 \simeq 0.4$ , and interpolating [62] it smoothly to measured (anti)neutrino structure functions  $F_{2,3}^{(\nu)N}(x, Q^2)$  by utilizing the CTEQ5 parametrization gives rise to a quicker power-like increase of  $(\nu)N$  cross sections at extremely high energies,  $E_\nu \gtrsim 10^8$  GeV, due to the power-like small- $x$  behavior implied by the DL-fit. This approach will be called [62] DL+CTEQ5 hereafter. The resulting  $\sigma_{\text{tot}}^{\nu N}(E_\nu)$  is shown in Fig. 7 and compared with our nominal (radiative GRV98 or CTEQ3-DIS) cross sections as well as with the somewhat smaller one corresponding to CTEQ4-DIS. The Regge ‘hard pomeron’ pole small- $x$  extrapolated DL+CTEQ5 cross section is, at highest energies, a factor of about 2 larger than our nominal cross section predicted by purely radiative QCD-RG evolutions which may be considered as a reasonable upper bound implied by a ‘conventional’ standard model approach. Similar remarks hold for the resulting downward  $\mu^+ + \mu^-$  event rates in Table 3 which should be compared with the nominal ones in Table 2: typically the Regge-inspired rates are enhanced by about 20%. It appears that yet much larger rates and cross sections than those in Table 3 and Fig. 7 are unlikely to be accommodated by currently conceivable standard model approaches and, if confirmed by future measurements, might require ‘new’ physics ideas for their explanation.

### 3 Event Rates for Surface Telescopes

For exploring the entire spectrum of cosmic neutrino fluxes up to highest neutrino energies of about  $10^{12}$  GeV in Fig. 1, large-area ground arrays and/or surface air fluorescence telescopes (like the Pierre Auger Observatory [28, 63] and the Telescope Array [26, 64]), where the interaction medium is not the Earth but the atmosphere, will become instrumental since upward-going neutrinos are essentially blocked by Earth for energies above  $10^8$  GeV. Here, near-horizontal incoming neutrinos will produce electromagnetic and/or hadronic extensive air showers which will be observed by Čerenkov radiation and/or fluorescence detectors. For a  $(\nu + \bar{\nu})$ -flux  $\Phi_{\nu+\bar{\nu}}$  reaching Earth, the event rate per second for deeply penetrating horizontal showers is given by [28, 26]

$$\text{rate}[E_{\text{sh}} > E_{\text{th}}] = N_A \rho_{\text{air}} \int_{E_{\text{th}}} dE_{\text{sh}} \int_0^1 dy \frac{d\Phi_{\nu+\bar{\nu}}(E_\nu)}{dE_\nu} \frac{d\sigma^{(\nu+\bar{\nu})N}(E_\nu, y)}{dy} \mathcal{A}(E_{\text{sh}}) \quad (3.1)$$

where  $\rho_{\text{air}} \simeq 10^{-3}$  g/cm<sup>3</sup> and  $\Phi_{\nu_\ell+\bar{\nu}_\ell} = \Phi/2$  for  $\ell = e, \mu, \tau$  and with the original  $\nu_\mu + \bar{\nu}_\mu$  flux  $\Phi$  at its production site given in Fig. 1 and the electron neutrino flux has been approximated by naive channel counting in pion production and decay ( $\nu_e/\nu_\mu = 1/2$ ) together with maximal mixing. The relation between the shower energy  $E_{\text{sh}}$  and the primary neutrino energy  $E_\nu$  depends on the neutrino interaction being considered and  $\mathcal{A}(E_{\text{sh}})$  is the (geometric) detector acceptance. If a detector just measures the shower energy (i.e. cannot distinguish between hadronic and electromagnetic showers) we have  $E_{\text{sh}} = E_\nu$  for  $(\nu_e+\bar{\nu}_e)N$  CC interactions, whereas  $E_{\text{sh}} = yE_\nu$  for  $(\nu_\mu+\bar{\nu}_\mu)N$  CC interactions where electromagnetic showers are negligible. This latter relation  $E_{\text{sh}} = yE_\nu$  holds also for all NC reactions which always produce hadronic showers. If a detector can distinguish between hadronic and electromagnetic showers this latter relation remains the same for all cases discussed except for  $(\nu_e+\bar{\nu}_e)N$  CC interactions where the neutrino energy has now to be shared between the hadronic and electromagnetic shower energy, i.e.  $E_{\text{sh,h}} = yE_\nu$  and  $E_{\text{sh,elm}} = (1-y)E_\nu$ . In Fig. 8 we display the relevant acceptances for the Auger detector [28] used for our calculations. We shall not employ the Auger acceptance as calculated

by Billoir [65] which has only been presented up to  $E_{\text{sh}} = 10^{10}$  GeV since we refrain from arbitrarily extrapolating [21] it to  $10^{12}$  GeV. The expected annual event rates are displayed in Table 4, employing the geometrical acceptances of Fig. 8. Utilizing instead the Monte Carlo simulated acceptance in Fig. 8 the resulting total (CC + NC) Auger rates would be about a factor of 3 smaller than the ones shown in Table 4. The largest event rates arise from  $(\nu_e + \bar{\nu}_e)N$  CC interactions, for which  $E_{\text{sh}} \simeq E_\nu$ . Therefore a measurement of the shower–energy dependence will shed some light on the theoretical cosmic neutrino flux models in Fig. 1 at ultrahigh energies  $E_\nu > 10^8$  GeV despite their decrease with increasing  $E_\nu$  which, in some cases (TD,  $Z$ –burst), is overcompensated by the increasing acceptances in Fig. 8. For example, quasi–horizontal air showers with  $E_{\text{sh}} > 10^8$  GeV will test the AGN–M95 flux dominantly at  $E_\nu \simeq 10^8 - 10^{10}$  GeV, the TD–SLBY flux at about  $10^9 - 10^{11}$  GeV and the  $Z$ –burst initiated flux at  $10^{10} - 10^{12}$  GeV according to the rates for the individual  $E_{\text{sh}}$ –bins in Table 4. Unfortunately the total amount of air–shower events is modest and in one year a few events may be observed in the Auger detector assuming modern estimates of AGN–M95, TD–SLBY and  $Z$ –burst neutrino fluxes. Most other cosmic neutrino flux models, in particular the recently updated and corrected GRB–WB flux [11], yield fractions of one event per year and remain undetectable by horizontal air showers. This situation remains practically unchanged even for the optimal Regge–inspired structure functions resulting in the largest  $\nu N$  cross section in Fig. 7 (event rates shown in parentheses in Table 4) which increase our nominal rates by less than 50%. (Our results agree of course with the total air shower rates estimated in [21, 28] when using the fluxes, structure functions and acceptances employed there.) Our total Auger results in Table 4 are compared, where available, with the expected total rates for the TA detector [26] which in some cases may be about a factor of 2 larger than for Auger.

Furthermore, contributions from  $\tau$ –neutrinos, with similar acceptances above  $10^8$  GeV as for  $\mu$ –neutrinos [26], may enhance the total air shower rates by as much as 20 to 30% [26]. We disregard such contributions here, partly because the appropriate detector

acceptances for  $\nu_\tau$  induced air showers do not exist in the literature, but mainly because Earth-skimming tau-neutrinos [42, 43, 25] will dominate over atmospheric interactions.

Tau-neutrinos when skimming the Earth [42, 43, 25] will be far more effective in producing, besides electromagnetic showers, specific double shower (‘double bang’) events. When ultrahigh energy cosmic neutrinos ( $E_\nu \gtrsim 10^8$  GeV) penetrate and skim the surface of Earth they convert to charged leptons which may leave the Earth’s surface essentially horizontally. For this to happen the neutrinos have to enter Earth near-horizontally at some critical nadir angle  $\theta(E_\nu)$ , typically [25, 26]  $\theta(E_\nu) \gtrsim 85^\circ$ , where they travel along chords with length of the order of their charged current interaction length  $\lambda_{\text{int}}^{CC}(E_\nu)$ . For larger nadir angles they rarely interact to produce charged leptons, whereas for smaller ones the neutrinos are shadowed by Earth. Electrons lose their energy too quickly in the Earth for being detected by ground-level surface telescopes. Furthermore, since  $\beta_\tau \simeq 0.8 \times 10^{-6}$  cm<sup>2</sup>/g  $\ll \beta_\mu \simeq 6.0 \times 10^{-6}$  cm<sup>2</sup>/g in the energy-loss relation (2.6), muons and taus can travel 1.5 km and 11 km, respectively, before losing a decade in energy [25, 48]. Thus, tau-neutrinos contribute dominantly to Earth-skimming events observed above the Earth’s surface which consist mainly of electromagnetic showers and of ‘double bang’ showers [25, 26, 42, 43]. The detected tau leptons determine the relevant total event rate which is given by [25]

$$N_\tau = 2 \int dE_\nu dE_\tau d\varphi d\cos\theta K(E_\nu, \theta; E_\tau) \frac{\cos\theta}{2\pi} \frac{d\Phi_{\nu_\tau}(E_\nu)}{dE_\nu} A_{\text{eff}}^\Omega(E_\tau) \text{TD} \quad (3.2)$$

for an isotropic neutrino flux  $\Phi_{\nu_\tau} = \Phi_{\bar{\nu}_\tau} = \Phi/4$ , according to the definition below Eq. (3.1), arriving with nadir angles  $\theta < \pi/2$  and the additional  $\cos\theta$  derives from projecting its trajectory (which nearly coincides with the  $\tau$ -trajectory for UHE  $\nu_\tau$ ’s) onto the surface area [66]. The probability (per  $E_\tau$ ) that a  $\nu_\tau$  entering Earth with energy  $E_\nu$  and nadir angle  $\theta$  produces a  $\tau$  that exits Earth with energy  $E_\tau$  is

$$K(E_\nu, \theta; E_\tau) \simeq N_A \sigma_{CC}^{\nu N}(E_\nu) \frac{1}{E_\tau \beta_\tau} \exp \left[ -N_A \sigma_{CC}^{\nu N}(E_\nu) \int_0^{2R_\oplus \cos\theta} dz' \rho(r(\theta, z')) \right] \\ \times \exp \left[ \frac{m_\tau}{c\tau_\tau \beta_\tau \rho_s} \left( \frac{1}{E_\nu} - \frac{1}{E_\tau} \right) \right] \quad (3.3)$$



with  $\rho(r)$  being the Earth density at distance  $r$  from its center (taken from Fig. 14 of [20]) with  $r^2(\theta, z) = R_{\oplus}^2 + z^2 - 2R_{\oplus}z \cos \theta$ ,  $R_{\oplus} \simeq 6371$  km, where  $z$  is the distance the incoming  $\nu_{\tau}$  travels through Earth before converting to a  $\tau$  near the Earth's surface where the density is  $\rho_s \simeq 2.65$  g/cm<sup>3</sup>. Furthermore,  $c\tau_{\tau} = 87.11$   $\mu\text{m}$  and  $m_{\tau} = 1777.03$  MeV. To account for the requirement of clear moonless nights for fluorescence detection, a duty cycle of 10% will be assumed in (3.2) as usual,  $D = 0.1$ , and the time  $T$  an experiment runs is taken, for convenience, to be 1 year although, once approved, the experiment will run for several years. For reasons discussed above, the integration over the nadir angle will be restricted to [25, 26]  $90^{\circ} - \theta \leq 5^{\circ}$  although the results do not depend too strongly on this specific choice. The factor of 2 in front of the integral in (3.2) accounts for the contribution of incoming antineutrinos since for  $E_{\nu} \gtrsim 10^8$  GeV the CC  $\nu_{\tau}$  and  $\bar{\nu}_{\tau}$  cross sections are virtually identical. The effective (geometrical) aperture  $A_{\text{eff}}^{\Omega}(E_{\tau})$  in (3.2) as estimated [25] for the TA detector (one station) is shown in Fig. 9 where for comparison the one for the far smaller HiRes detector is shown as well. The sensitivity of the fluorescence detectors of the Auger Observatory is expected [25] to lie somewhere between that of HiRes and TA in Fig. 9, but such a quantity has unfortunately not yet been separately published.

The nominal event rate (based on our GRV98 or CTEQ3–DIS parton densities) for the six neutrino sources given in Fig. 1, binned by the  $\tau$ –energy, are given in Table 5 for the TA detector assuming 10 observational stations [26]. (We refrain from recalculating the rates for the Fly's Eye and HiRes detectors which have been shown to be marginal [25].) The expected rates for the largest Regge–inspired  $\nu N$  cross section (cf. Fig. 7) are shown in parentheses which are in most cases smaller than the nominal ones (based on GRV98 or CTEQ3–DIS in Fig. 7) since the first (attenuation) exponential in (3.3) becomes dominant for  $E_{\nu} \gtrsim 10^9$  GeV even for the rather small column depth involved. This implies that if event rates are calculated utilizing even smaller UHE  $\nu N$  cross sections than the ones in Fig. 7 (due to flatter and thus less steep extrapolations to the ultrasmall Bjorken–

$x$  region  $x \sim M_W^2/s$  of conventionally fitted parton densities), one easily overestimates Earth-skimming rates at highest energies. For comparison the total TA event rates as estimated in [26] are, where available, shown as well which are somewhat smaller than our results and the ones obtained in [25]. This is presumably due to the fact that the realistic TA aperture is expected to be somewhat smaller [67] than the one calculated in [25] and shown in Fig. 9 because of effects such as the detector response, light propagation in air and night sky background. The total rates for the Auger detector are also shown in Table 5 which we have calculated for our neutrino fluxes in Fig. 1 using the effective Auger aperture [43] where, besides the dominant electromagnetic showers, multi-bang events have been also taken into account for the Monte Carlo simulations (for definiteness we used the average aperture in Fig. 9 of [43] as obtained from the ‘BS+PP+DIS low’ continuous energy loss model). In any case, in contrast to the quasi-horizontal air showers in Table 4, the shower event rates produced by Earth-skimming  $\nu_\tau$ ’s are sufficiently large for testing and exploring the large energy tail ( $\gtrsim 10^8$  GeV) up to  $10^{11}$  GeV of most cosmic neutrino sources in Fig. 1, except for the recently updated and corrected GRB-WB flux [11] for which the rates remain prohibitively small.

In order to learn to what extent the shower rates measured in certain bins of  $E_\tau$  as shown in Table 5 can explore and test the energy profile of the theoretical cosmic neutrino fluxes  $\Phi(E_\nu)$  in Fig. 1, we display in Table 6 the individual  $E_\nu$ -binned contributions to our nominal TA-rates for the  $E_\tau$ -bins given in Table 5 for three representative neutrino fluxes. Apart from the less steep falling  $Z$ -burst flux in Fig. 1 which contributes over a wider  $E_\nu$ -range for a given  $E_\tau$ -bin, measured showers with  $E_\tau = 10^8 - 10^9$  GeV will test cosmic neutrino fluxes mainly within  $E_\nu = 10^8 - 10^{10}$  GeV, whereas increasing the shower energy to  $E_\tau = 10^9 - 10^{10}$  GeV, for example, will delineate a similar  $E_\nu$ -bin,  $E_\nu = 10^9 - 10^{10}$  GeV. The same holds true for even higher values of  $E_\tau$ . Therefore from an experimental point of view it will be important to measure the detailed energy ( $E_\tau$ ) dependence predicted in Table 5 for exploring cosmic neutrino sources at highest energies.

## 4 Implications of Low Scale ‘Extra Dimensions’

Having calculated so far in the previous Section the muon and shower event rates caused by extragalactic neutrinos according to conventional (nominal) and optimal (Regge inspired) standard model expectations, we will now finally give for comparison a few examples of distinctively different event rates which derive from ‘new’ physics ideas. Although highly speculative and by far non-unique, let us choose string theories with large ‘extra dimensions’  $\delta$  where only gravity propagates in the  $4 + \delta$  dimensional bulk of spacetime (a recent brief review can be found in [68]). To obtain the effective low-energy theory in  $3 + 1$  dimensions, these extra dimensions are compactified to a common scale  $R$  which may be relatively large, corresponding to a small scale  $1/R$  of new physics, and is related to standard Newton gravity (Planck scale) via  $G_N^{-1} \sim M_S^{\delta+2} R^\delta$  with  $M_S \sim \text{TeV}$  being the low energy effective string scale [69]. (For example,  $R$  is of the order of 1 mm for  $\delta = 2$ .) In addition to the usual Standard Model (SM) particles, an infinite tower of massive Kaluza-Klein (KK) excitations appears in the effective four-dimensional theory, corresponding to the massless graviton in  $4 + \delta$  dimensions, and  $M_S$  plays the role of an ultraviolet cutoff for the summation over all relevant spin-2 KK states. Such a scenario opens up the interesting possibility of massive spin-2  $t$ -channel exchange which results in a more rapid growth with energy as compared to SM cross sections derived from massive vector boson exchange considered thus far. Being flavor-neutral this ‘graviton’ KK exchange ( $G$ ) contributes only via NC processes to the total SM  $\nu N$  cross section. The cross sections for the partonic subprocesses  $\nu q \rightarrow \nu q^{(-)}$  and  $\nu g \rightarrow \nu g$  as mediated by  $G$  read [58, 59, 70, 69]

$$\frac{d\hat{\sigma}_G^{(-)\nu q}}{d\hat{t}} = \frac{\pi}{32M_S^8} \frac{1}{\hat{s}^2} [32\hat{s}^4 + 64\hat{s}^3\hat{t} + 42\hat{s}^2\hat{t}^2 + 10\hat{s}\hat{t}^3 + \hat{t}^4] F(\hat{s}, \hat{t}) \quad (4.1)$$

$$\frac{d\hat{\sigma}_G^{\nu g}}{d\hat{t}} = \frac{\pi}{2M_S^8} \frac{1}{\hat{s}^2} [2\hat{s}^4 + 4\hat{s}^3\hat{t} + 3\hat{s}^2\hat{t}^2 + \hat{s}\hat{t}^3] F(\hat{s}, \hat{t}) \quad (4.2)$$

for  $\delta = 2$  extra dimensions and the terms in square brackets are symmetric under  $\hat{s} \leftrightarrow \hat{t}$ . The function  $F(\hat{s}, \hat{t})$  refers to some unitarization (interpolation) procedure [58, 59, 71] in

order to extrapolate the perturbative predictions at  $\hat{s} \lesssim M_S^2$  in (4.1) and (4.2) to  $\hat{s} \gg M_S^2$ . We shall use two representative choices [58],

$$F(\hat{s}, \hat{t}) = \frac{M_S^6}{(M_S^2 + \hat{s})^2(M_S^2 - \hat{t})} [1 + 10 \ln(1 + \hat{s}/M_S^2)] \quad (4.3)$$

$$F(\hat{s}, \hat{t}) = \frac{M_S^4}{(M_S^2 + \hat{s})(M_S^2 - \hat{t})} \quad (4.4)$$

as well as choosing  $M_S = 1$  TeV for our subsequent quantitative analysis. The contribution to the total SM  $\nu N$  cross section due to ‘graviton’ KK exchange is thus given by

$$\frac{d\sigma_G^{\nu N}}{dx dy} = s \sum_{f=q, \bar{q}, g} x f(x, Q^2) \frac{d\hat{\sigma}_G^{\nu f}}{d\hat{t}} \quad (4.5)$$

with  $\hat{s} = xs$ ,  $\hat{t} = t \equiv -Q^2 = -xys$  and only the dominant light quarks  $q = u, d, s$  are taken into account. The same expression holds for  $\bar{\nu}N$  scattering. In Fig. 10 our nominal SM total (CC + NC)  $\nu N$  cross section is compared with the additional KK contribution where the dominant gluon initiated component in (4.5) is, at highest energies, about a factor of 2 to 4 larger than the sea contributions of (anti)quarks depending on whether the interpolation (4.4) or (4.3), respectively, is used. (It should be noticed that these cross sections are in agreement with the upper bound derived in [72]. A more recent updated estimate [73], however, being based on the full exposure of the AGASA and Fly’s Eye experiments as well as on a larger cosmogenic neutrino flux [74] together with a larger nucleon source cutoff energy, would rule out the largest strongly rising cross section (dashed curve) in Fig. 10 at highest neutrino energies.) These total SM + KK  $\nu N$  cross sections can rise to hadronic mb-scale values [58, 59] at highest neutrino energies and the resulting annual total event rates for the relevant quasi-horizontal air showers, shown in Table 7, are enormous when compared with the small SM rates in Table 4. Even for highest neutrino energies (i.e. highest threshold energies in (3.1)) the number of events remains large, except for the steeply falling AGN-SS and GRB-WB fluxes in Fig. 1. It should be easy for the future Pierre Auger Observatory to observe such dramatically large hadronic shower event rates as implied by low-scale large ‘extra dimension’ scenarios.

(Given the uncertainties in the cosmic neutrino flux predictions, the eventual detection of such event rates will be subject to interpretation, because they are proportional to the product of the flux and the cross section. Ways to discriminate between large neutrino cross sections and large neutrino fluxes have been suggested recently by looking at the zenith angle distribution of the neutrino induced shower events, i.e. by comparing the energy spectrum of upgoing and nearly horizontal to downgoing shower events [66, 75]. Such a measurement may at least in principle allow to determine  $\sigma^{(\nu+\bar{\nu})N}$  independently of the neutrino flux.) The viability of such ‘new’ physics scenarios may be even tested by the smaller ground level AGASA [76] and Fly’s Eye (HiRes) [77] observatories: using their estimated shower acceptances [78, 77], the expected rates for AGASA are about a factor of 25 smaller than the ones in Table 7, and a similar reduction holds for the Fly’s Eye (HiRes) observatory.

## 5 Summary

In order to explore and test the sources of cosmic UHE neutrinos, the calculation of the relevant  $\overset{(-)}{\nu}N$  cross sections requires the knowledge of parton distributions  $f(x, Q^2)$ , with  $f = q, \bar{q}, g$ , at ultrasmall Bjorken  $x \sim M_W^2/s$ , below the range constrained by present experiments, and at scales  $Q^2 = M_W^2$ . Highest neutrino energies  $E_\nu = s/2M_N \simeq 10^{12}$  GeV require extrapolations down to  $x \simeq 10^{-9}$ . Within standard QCD RG–evolutions, such extensive small– $x$  extrapolations can be uniquely and reliably predicted by the dynamical (radiative) parton model [32] which proved to provide reliable high energy small– $x$  predictions in the past. (Interestingly, consistent BFKL model resummations in leading order QCD yield remarkably similar results [35].) All resulting relevant  $\overset{(-)}{\nu}N$  cross sections turn out to have a typical uncertainty of about  $\pm 20\%$  at highest neutrino energies of  $10^{12}$  GeV [36]. We have adopted this ‘nominal’ approach for all our calculations which are based on the canonical radiative GRV98 parton distributions [32]. Similar results are

accidentally obtained from the conventionally fitted CTEQ3–DIS parametrizations [37] at  $x \gtrsim 10^{-5}$  with their assumed fixed–power extrapolation to  $x < 10^{-5}$ , whereas the CTEQ4–DIS parametrizations [38] somewhat underestimate the neutrino–nucleon cross sections by about 20% at  $E_\nu \simeq 10^{10} - 10^{12}$  GeV. In calculating event rates caused by cosmic UHE neutrinos we have also employed recent Regge–model inspired small– $x$  structure functions [61, 62] in order to learn about possible maximal rates which may be accommodated by ‘conventional’ standard model approaches and which do not necessarily require ‘new’ physics interpretations.

For the representative set of modern cosmic neutrino fluxes in Fig. 1 we first analyzed  $\mu^+ + \mu^-$  event rates caused by upward–going UHE neutrinos for modern (future) underground detectors (such as ANTARES, AMANDA II and IceCube), with special emphasis on NC regeneration effects which populate the lower energy part of the attenuated flux spectra. Regeneration increases the non–regenerated event rates [20, 21, 23] on the average by as much as 20%. In particular AGN models, yielding the highest signal rates, might be testable in this way for neutrino energies as large as  $10^7 - 10^8$  GeV, i.e. well above  $10^5$  GeV where the atmospheric neutrino background becomes marginal. In addition we demonstrated in detail in Table 1 to what extent high– $E_\nu$  bins of the original fluxes in Fig. 1 remain experimentally accessible after their depletion and regeneration due to NC interactions. Measurements of these energy–dependencies will be crucial for exploring the nature of various cosmic neutrino sources.

In contrast to these upward  $\mu^+ + \mu^-$  rates, the downward–going muon rates depend strongly on the specific choice of parton distributions and would allow to test cosmic neutrino fluxes at higher  $E_\nu$  (about a factor of 10 higher than for the upward rates, cf. Table 2), provided that downward–going muons, produced by interactions within the instrumented volume, can be observed efficiently. The largest Regge–inspired cross section(s) in Fig. 7 give rise to downward  $\mu^+ + \mu^-$  event rates (Table 3) which are about 20 – 30% larger than our nominal ones in Table 2, and may be considered as reasonable upper

bounds of present standard model approaches.

To explore the entire spectrum of cosmic neutrino fluxes up to highest neutrino energies of about  $10^{12}$  GeV, one has to resort to quasi–horizontal air showers and Earth–skimming  $\nu_\tau$ ’s to be detected by large area ground arrays and surface air fluorescence telescopes (such as the Pierre Auger Observatory and the Telescope Array), since upward–going neutrinos are essentially blocked by Earth for energies above  $10^8$  GeV. The detailed shower energy  $E_{\text{sh}}$  dependence, which practically coincides with the one of the incoming cosmic neutrinos, of the annual event rates for the Auger detector has been presented in Table 4 as well as the results derived from the largest Regge inspired cross sections which can be at most 50% larger than our nominal rates. The most efficient way, however, to test cosmic neutrino fluxes at highest energies,  $10^8 \lesssim E_\nu \lesssim 10^{11}$  GeV, will be Earth–skimming tau–neutrinos [42, 43, 25] which, when converting to  $\tau$ –leptons that escape Earth, produce dominantly near–horizontal electromagnetic showers as well as specific ‘double–bang’ events. Our nominal rates are presented, for various bins in  $E_\tau$ , in Table 5 and compared with the expected rates for the Auger detector. Here the largest Regge–inspired  $\nu N$  cross section (cf. Fig. 7) implies in most cases smaller rates than our nominal ones (based on GRV98 or CTEQ3–DIS) since the attenuation (absorption) exponential in (3.3) becomes dominant at neutrino energies above  $10^9$  GeV despite the rather small column depth involved. In order to learn to what extent the measured shower rates in certain bins of  $E_\tau$  will be able to delineate specific features of the energy profile of the various theoretical cosmic neutrino fluxes  $\Phi(E_\nu)$  in Fig. 1, we presented in Table 6 the individual  $E_\nu$ –binned contributions to the nominal TA–rates for given  $E_\tau$ –bins. In any case it will be important to measure the detailed energy ( $E_{\text{sh}}$  and  $E_\tau$ ) dependencies for exploring extragalactic neutrino sources at highest energies of  $10^{21}$  eV.

Finally, as an illustration of possible implications of ‘new’ physics, we calculated highly speculative expectations of string scenarios with large ‘extra dimensions’ at low TeV–scales. The additional contributions, due to the exchange of massive ‘graviton’ spin–2

Kaluza–Klein excitations in neutral current neutrino–quark (gluon) scattering to the relevant quasi–horizontal hadronic air showers may be enormous as compared with the moderate SM event rates for the Auger detector and could be detected in the not too distant future. The viability of such ‘new’ physics scenarios may be tested even by the smaller ground level AGASA and Fly’s Eye (HiRes) detectors.

## Acknowledgements

We thank M. Glück for many helpful discussions as well as for his collaboration at the initial stage of this work, and P. Billoir for a clarifying correspondence. We are also indebted to S.I. Yanush for providing us with the computer code of the Regge–inspired DL+CTEQ5 structure functions. This work has been supported in part by the ‘Bundesministerium für Bildung und Forschung’, Berlin/Bonn.



## References

- [1] R. J. Protheroe, Nucl. Phys. Proc. Suppl. **77** (1999) 465.
- [2] F. Halzen, Phys. Rept. **333** (2000) 349.
- [3] D. B. Cline and F. W. Stecker, astro-ph/0003459.
- [4] A. V. Olinto, astro-ph/0102077;  
P. Blasi, astro-ph/0110401.
- [5] G. Sigl, hep-ph/0109202;  
P. Bhattacharjee and G. Sigl, Phys. Rept. **327** (2000) 109 [astro-ph/9811011].
- [6] K. Greisen, Phys. Rev. Lett. **16** (1966) 748;  
G. T. Zatsepin and V. A. Kuzmin, JETP Lett. **4** (1966) 78 [Pisma Zh. Eksp. Teor. Fiz. **4** (1966) 114].
- [7] F. W. Stecker, Astrophys. J. **228** (1979) 919.
- [8] K. Mannheim, Astropart. Phys. **3** (1995) 295.
- [9] F. W. Stecker and M. H. Salamon, Space Sci. Rev. **75** (1996) 341 [astro-ph/9501064].
- [10] F. Halzen and E. Zas, Astrophys. J. **488** (1997) 669 [astro-ph/9702193].
- [11] E. Waxman and J. N. Bahcall, Phys. Rev. D **59** (1999) 023002 [hep-ph/9807282].
- [12] R. J. Protheroe and T. Stanev, Phys. Rev. Lett. **77** (1996) 3708; [Erratum ibid. **78** (1997) 3420] [astro-ph/9605036].
- [13] V. Berezhinsky, M. Kachelriess and A. Vilenkin, Phys. Rev. Lett. **79** (1997) 4302 [astro-ph/9708217];  
M. Birkel and S. Sarkar, Astropart. Phys. **9** (1998) 297 [hep-ph/9804285];

- Z. Fodor and S. D. Katz, Phys. Rev. Lett. **86** (2001) 3224 [hep-ph/0008204];
- S. Sarkar and R. Toldra, Nucl. Phys. B **621** (2002) 495 [hep-ph/0108098];
- C. Barbot and M. Drees, Phys. Lett. B **533** (2002) 107 [hep-ph/0202072].
- [14] G. Sigl, S. Lee, D. N. Schramm and P. Coppi, Phys. Lett. B **392** (1997) 129 [astro-ph/9610221].
- [15] G. Sigl, S. Lee, P. Bhattacharjee and S. Yoshida, Phys. Rev. D **59** (1999) 043504 [hep-ph/9809242].
- [16] U. F. Wichoski, J. H. MacGibbon and R. H. Brandenberger, Phys. Rev. D **65** (2002) 063005 [hep-ph/9805419].
- [17] T. J. Weiler, Phys. Rev. Lett. **49** (1982) 234; Astropart. Phys. **11** (1999) 303 [hep-ph/9710431]; Astropart. Phys. **12** (2000) 379 (E);
- D. Fargion, B. Mele and A. Salis, Astrophys. J. **517** (1999) 725.
- [18] S. Yoshida, G. Sigl and S. Lee, Phys. Rev. Lett. **81** (1998) 5505 [hep-ph/9808324].
- [19] L.V. Volkova, Yad. Fiz. **31** (1980) 1510, [Sov. J. Nucl. Phys. **31** (1980) 784].
- [20] R. Gandhi, C. Quigg, M. H. Reno and I. Sarcevic, Astropart. Phys. **5** (1996) 81 [hep-ph/9512364].
- [21] R. Gandhi, C. Quigg, M. H. Reno and I. Sarcevic, Phys. Rev. D **58** (1998) 093009 [hep-ph/9807264].
- [22] G. M. Frichter, D. W. McKay and J. P. Ralston, Phys. Rev. Lett. **74** (1995) 1508 [Erratum *ibid.* **77** (1996) 4107] [hep-ph/9409433].
- [23] G. C. Hill, Astropart. Phys. **6** (1997) 215 [astro-ph/9607140].
- [24] C. Hettlage and K. Mannheim, Proc. 2nd Workshop on Methodical Aspects of Underwater/Underice Neutrino Telescopes, Hamburg, 2001, astro-ph/0202074.

- [25] J. L. Feng, P. Fisher, F. Wilczek and T. M. Yu, Phys. Rev. Lett. **88** (2002) 161102 and MIT-CTP-3122 [hep-ph/0105067].
- [26] M. Sasaki, Y. Asaoka and M. Jobashi, Univ. Tokyo ICRR-Report-484-2002-2 [astro-ph/0204167 v2].
- [27] G. Parente and E. Zas, Proc. 7th Int. Symp. Neutrino Telescopes, Venice, Italy, Feb. 1996, p.499 [astro-ph/9606091].
- [28] K. S. Capelle, J. W. Cronin, G. Parente and E. Zas, Astropart. Phys. **8** (1998) 321 [astro-ph/9801313].
- [29] M. Glück, E. Reya and A. Vogt, Z. Phys. C **48** (1990) 471.
- [30] M. Glück, E. Reya and A. Vogt, Z. Phys. C **53** (1992) 127, Phys. Lett. B **306** (1993) 391.
- [31] M. Glück, E. Reya and A. Vogt, Z. Phys. C **67** (1995) 433.
- [32] M. Glück, E. Reya and A. Vogt, Eur. Phys. J. C **5** (1998) 461 [hep-ph/9806404].
- [33] I. Abt *et al.* [H1 Collaboration], Nucl. Phys. B **407** (1993) 515; T. Ahmed *et al.*, Nucl. Phys. B **439** (1995) 471; S. Aid *et al.*, Phys. Lett. B **354** (1995) 494; M. Derrick *et al.* [ZEUS Collaboration], Phys. Lett. B **316** (1993) 412; Z. Phys. C **65** (1995) 379; Phys. Lett. B **345** (1995) 576.
- [34] S. Aid *et al.* [H1 Collaboration], Nucl. Phys. B **470** (1996) 3; C. Adloff *et al.*, Nucl. Phys. B **497** (1997) 3; M. Derrick *et al.* [ZEUS Collaboration], Z. Phys. C **69** (1996) 607; Z. Phys. C **72** (1996) 399.
- [35] J. Kwiecinski, A. D. Martin and A. M. Stasto, Phys. Rev. D **59** (1999) 093002 [astro-ph/9812262].

- [36] M. Glück, S. Kretzer and E. Reya, *Astropart. Phys.* **11** (1999) 327 [astro-ph/9809273].
- [37] H. L. Lai *et al.*, CTEQ3, *Phys. Rev. D* **51** (1995) 4763 [hep-ph/9410404].
- [38] H. L. Lai *et al.*, CTEQ4, *Phys. Rev. D* **55** (1997) 1280 [hep-ph/9606399].
- [39] E. Aslanides *et al.* [ANTARES Collaboration], astro-ph/9907432.
- [40] M. Nagano and A. A. Watson, *Rev. Mod. Phys.* **72** (2000) 689.
- [41] X. Bertou, M. Boratav and A. Letessier-Selvon, *Int. J. Mod. Phys. A* **15** (2000) 2181 [astro-ph/0001516].
- [42] D. Fargion, *Astrophys. J.* **570** (2002) 909 [astro-ph/0002453]; hep-ph/0111289 v2.
- [43] X. Bertou, P. Billoir, O. Deligny, C. Lachaud and A. Letessier-Selvon, *Astropart. Phys.* **17** (2002) 183 [astro-ph/0104452].
- [44] A. Nicolaidis and A. Taramopoulos, *Phys. Lett. B* **386** (1996) 211 [hep-ph/9603382].
- [45] V. A. Naumov and L. Perrone, *Astropart. Phys.* **10** (1999) 239 [hep-ph/9804301].
- [46] D. E. Groom *et al.* [Particle Data Group Collaboration], *Eur. Phys. J. C* **15** (2000) 1, pp 152.
- [47] A. Dar, J. J. Lord and R. J. Wilkes, *Phys. Rev. D* **33** (1986) 303.
- [48] P. Lipari and T. Stanev, *Phys. Rev. D* **44** (1991) 3543.
- [49] A. M. Dziewonski and D. L. Anderson, “Preliminary Reference Earth Model”, *Phys. Earth Planet. Interiors* **25** (1981) 297.
- [50] A. Biron *et al.*, ”Proposal Upgrade of AMANDA-B towards AMANDA-II”, DESY-Zeuthen report (1997)

- [51] M. Leuthold, “Ice Cube Configuration Studies”, *Prepared for International Workshop on Simulations and Analysis Methods for Large Neutrino Telescopes, DESY–Zeuthen, Germany, 6-9 Jul 1998*
- [52] S. Fukuda *et al.* [Super-Kamiokande Collaboration], Phys. Rev. Lett. **85** (2000) 3999 [hep-ex/0009001]; Phys. Rev. Lett. **86** (2001) 5656 [hep-ex/0103033].
- [53] J. G. Learned and S. Pakvasa, Astropart. Phys. **3** (1995) 267 [hep-ph/9405296].
- [54] H. Athar, M. Jezabek and O. Yasuda, Phys. Rev. D **62** (2000) 103007 [hep-ph/0005104];  
L. Bento, P. Keränen and J. Maalampi, Phys. Lett. B **476** (2000) 205 [hep-ph/9912240].
- [55] J. Alvarez-Muniz, F. Halzen and D. W. Hooper, Phys. Rev. D **62** (2000) 093015 [astro-ph/0006027].
- [56] S. I. Dutta, M. H. Reno and I. Sarcevic, Phys. Rev. D **62** (2000) 123001 [hep-ph/0005310]; Phys. Rev. D **64** (2001) 113015 [hep-ph/0104275].
- [57] S. Bottai and S. Giurgola, Astropart. Phys. **18** (2003) 539 [astro-ph/0205325].
- [58] P. Jain, D. W. McKay, S. Panda and J. P. Ralston, Phys. Lett. B **484** (2000) 267 [hep-ph/0001031].
- [59] M. Kachelriess and M. Plümacher, Phys. Rev. D **62** (2000) 103006 [astro-ph/0005309].
- [60] F. Cornet, J. I. Illana and M. Masip, Phys. Rev. Lett. **86** (2001) 4235 [hep-ph/0102065].
- [61] A. Donnachie and P. V. Landshoff, Phys. Lett. B **437** (1998) 408 [hep-ph/9806344]; Phys. Lett. B **518** (2001) 63 [hep-ph/0105088].

- [62] V. S. Berezinsky, A. Z. Gazizov and S. I. Yanush, Phys. Rev. D **65** (2002) 093003 [astro-ph/0105368].
- [63] Auger Collaboration, "The Pierre Auger Project Design Report", FERMILAB-PUB-96-024, Feb. 1997, <http://www.auger.org>.
- [64] TA Collaboration, "The Telescope Array Project Design Report", July 2000, <http://www-ta.icrr.u-tokyo.ac.jp>
- [65] P. Billoir, Pierre Auger project note GAP-97-049, L.P.N.H.E. Paris VI-VII ([http://www.auger.org/admin-cgi-bin/woda/gap\\_notes.pl](http://www.auger.org/admin-cgi-bin/woda/gap_notes.pl))
- [66] A. Kusenko and T. J. Weiler, Phys. Rev. Lett. **88** (2002) 161101 [hep-ph/0106071].
- [67] Y. Asaoka, M. Jobashi and M. Sasaki, private communication.
- [68] Particle Data Group, J. Hewett and J. March-Russell, Phys. Rev. D **66** (2002) 010001-945, and references therein.
- [69] T. Han, J. D. Lykken and R.-J. Zhang, Phys. Rev. D **59** (1999) 105006 [hep-ph/9811350];  
G. F. Giudice, R. Rattazzi and J. D. Wells, Nucl. Phys. B **544** (1999) 3 [hep-ph/9811291].
- [70] P. Mathews, S. Raychaudhuri and K. Sridhar, Phys. Lett. B **455** (1999) 115 [hep-ph/9812486].
- [71] S. Nussinov and R. Shrock, Phys. Rev. D **59** (1999) 105002 [hep-ph/9811323].
- [72] C. Tyler, A.V. Olinto and G. Sigl, Phys. Rev. **D63** (2001) 055001 [hep-ph/0002257].
- [73] L.A. Anchordoqui, J.L. Feng, H. Goldberg and A.D. Shapere, Phys. Rev. **D66** (2002) 103002 [hep-ph/0207139 v2].
- [74] O.E. Kalashev *et al.*, Phys. Rev. **D66** (2002) 063004.

- [75] J. Alvarez-Muñiz, F. Halzen, T. Han and D. Hopper, Phys. Rev. Lett. **88** (2002) 021301.
- [76] S. Yoshida *et al.*, Astropart. Phys. **3** (1995) 105; [www.icrr.u-tokyo.ac.jp/as/project/agasa.html](http://www.icrr.u-tokyo.ac.jp/as/project/agasa.html)
- [77] D. J. Bird *et al.* [HIRES Collaboration], Astrophys. J. **424** (1994) 491; <http://hires.physics.utha.edu>; T. Abu-Zayyad *et al.* [High Resolution Fly's Eye Collaboration], astro-ph/0208243 v2.
- [78] L. A. Anchordoqui, J. L. Feng, H. Goldberg and A. D. Shapere, Phys. Rev. D **65** (2002) 124027 [hep-ph/0112247].

Table 1: Total upward  $\mu^+ + \mu^-$  event rates per year from  $\nu_\mu N$  and  $\bar{\nu}_\mu N$  interactions in rock calculated according to (2.1) for various muon energy thresholds  $E_\mu^{min}$  and the appropriate cosmic neutrino fluxes in Fig.1. The numbers in parentheses refer to the event rates with no regeneration, i.e.  $\Psi \equiv 1$  in (2.10). The background ATM rates are shown for comparison.

flux	detector	muon-energy threshold $E_\mu^{min}/\text{GeV}$				
		$10^3$	$10^4$	$10^5$	$10^6$	$10^7$
ATM	ANTARES	498 (490)	16.92 (16.62)	0.20 (0.20)	0.001 (0.001)	-
	AMANDA-II	1362 (1352)	37.8 (36.8)	0.34 (0.32)	0.0016 (0.0014)	-
	IceCube	8860 (8800)	163.4 (159)	1.3 (1.2)	0.006 (0.006)	-
AGN-SS	ANTARES	411 (359)	248 (215)	89.3 (76.1)	13.0 (10.8)	0.53 (0.45)
	AMANDA-II	699 (612)	408 (355)	137 (116)	19.3 (16.1)	0.79 (0.67)
	IceCube	2687 (2356)	1547 (1346)	514 (439)	72.6 (60.7)	3.00 (2.53)
AGN-M95	ANTARES	13.7 (12.6)	5.00 (4.30)	1.98 (1.61)	0.90 (0.72)	0.32 (0.26)
	AMANDA-II	29.1 (27.2)	8.62 (7.55)	2.98 (2.42)	1.34 (1.07)	0.46 (0.38)
	IceCube	143 (135)	33.7 (29.5)	11.2 (9.11)	5.04 (4.05)	1.74 (1.43)
GRB-WB	ANTARES	0.60 (0.54)	0.32 (0.28)	0.08 (0.07)	0.010 (0.008)	0.0003 (0.0003)
	AMANDA-II	1.10 (1.00)	0.56 (0.50)	0.13 (0.11)	0.015 (0.012)	0.0005 (0.0004)
	IceCube	4.35 (3.94)	2.13 (1.91)	0.49 (0.42)	0.055 (0.046)	0.0018 (0.0015)
TD-SLBY	ANTARES	0.62 (0.51)	0.45 (0.36)	0.26 (0.21)	0.12 (0.098)	0.045 (0.037)
	AMANDA-II	0.97 (0.80)	0.68 (0.56)	0.39 (0.32)	0.18 (0.145)	0.067 (0.054)
	IceCube	3.70 (3.06)	2.57 (2.11)	1.47 (1.19)	0.68 (0.550)	0.250 (0.210)
TD-SLSC	ANTARES	0.006 (0.005)	0.005 (0.004)	0.003 (0.003)	0.002 (0.002)	0.001 (0.001)
	AMANDA-II	0.010 (0.008)	0.007 (0.006)	0.005 (0.004)	0.003 (0.003)	0.002 (0.001)
	IceCube	0.036 (0.030)	0.028 (0.022)	0.020 (0.015)	0.012 (0.001)	0.006 (0.005)
Z-burst	ANTARES	0.008 (0.007)	0.007 (0.006)	0.006 (0.005)	0.005 (0.004)	0.003 (0.003)
	AMANDA-II	0.013 (0.010)	0.011 (0.009)	0.009 (0.007)	0.007 (0.005)	0.005 (0.004)
	IceCube	0.047 (0.038)	0.041 (0.032)	0.033 (0.026)	0.026 (0.020)	0.019 (0.015)



Table 2: Total downward  $\mu^+ + \mu^-$  event rates per year arising from  $\nu_\mu N$  and  $\bar{\nu}_\mu N$  interactions in a detector with an effective volume  $V_{eff} = A_{eff} \times 1\text{km} = 1\text{km}^3$  of water calculated according to (2.3) with  $S \equiv 1$  for various muon energy thresholds  $E_\mu^{min}$ . The background ATM rates are shown for comparison.

flux	$E_\mu^{min}$ [GeV]					
	$10^5$	$10^6$	$10^7$	$10^8$	$10^9$	$10^{10}$
ATM	5.08	0.041	$3 \times 10^{-4}$	-	-	-
AGN-SS	510	207	30.9	0.34	$1.0 \times 10^{-4}$	-
AGN-M95	11.8	8.95	7.09	3.74	0.88	0.054
GRB-WB	0.61	0.16	0.02	$5 \times 10^{-4}$	-	-
TD-SLBY	1.47	1.30	1.00	0.63	0.30	0.10
TD-SLSC	0.028	0.027	0.025	0.022	0.017	0.010
Z-burst	0.082	0.082	0.082	0.081	0.077	0.063

Table 3: Total downward  $\mu^+ + \mu^-$  event rates per year for a detector with  $V_{eff} = 1\text{km}^3$  as in Table 2 but using the DL+CTEQ5 structure functions [62] with their Regge model inspired small-x extrapolation [61]. The background ATM rates are shown for comparison.

flux	$E_\mu^{min}$ [GeV]					
	$10^5$	$10^6$	$10^7$	$10^8$	$10^9$	$10^{10}$
ATM	5.69	0.047	$3 \times 10^{-4}$	-	-	-
AGN-SS	586	241	35.9	0.40	$1.0 \times 10^{-4}$	-
AGN-M95	13.8	10.5	8.35	4.45	1.09	0.072
GRB-WB	0.70	0.19	0.02	$6 \times 10^{-4}$	-	-
TD-SLBY	1.75	1.55	1.21	0.77	0.38	0.13
TD-SLSC	0.036	0.035	0.033	0.029	0.023	0.015
Z-burst	0.116	0.115	0.115	0.114	0.109	0.091

Table 4: Total annual event rates for the Pierre Auger Observatory for horizontal air showers induced by  $(\nu_e + \bar{\nu}_e)N$  and  $(\nu_\mu + \bar{\nu}_\mu)N$  CC and NC interactions calculated according to (3.1) using the geometrical acceptances of Fig.8 and the appropriate cosmic neutrino fluxes of Fig.1. The numbers in parentheses refer to the rates as obtained by using the (optimal) DL+CTEQ5 structure functions [62] with their Regge model inspired small-x extrapolation [61]. For comparison the expected rates for the Telescope Array are also displayed, where available, which have been estimated [26] using CTEQ4-DIS parton distributions and assuming a duty cycle of 0.1 for observing the atmospheric fluorescence light.

flux	$E_{sh}(\text{GeV})$	detectors			TA		
		Auger	Auger	Auger	CC( $\nu_e, \nu_\mu$ )	NC	total
		CC( $\nu_e, \nu_\mu$ )	NC	total			
AGN-SS	$10^8 - 10^9$	0.032 (0.039)	0.007 (0.008)	0.039 (0.047)			
	$10^9 - 10^{10}$	0.0001 (0.0001)	0.000008 (0.000009)	0.0001 (0.0001)			
	$10^{10} - 10^{11}$	– (–)	– (–)	– (–)	–		
	$10^{11} - 10^{12}$	– (–)	– (–)	– (–)	–		
	total	0.032 (0.039)	0.007 (0.008)	0.039 (0.047)	–	–	–
AGN-M95	$10^8 - 10^9$	1.42 (1.78)	0.57 (0.64)	1.99 (2.42)			
	$10^9 - 10^{10}$	1.52 (1.97)	0.27 (0.33)	1.79 (2.30)			
	$10^{10} - 10^{11}$	0.19 (0.27)	0.015 (0.02)	0.21 (0.29)	–		
	$10^{11} - 10^{12}$	– (–)	– (–)	–			
	total	3.13 (4.02)	0.86 (0.99)	3.99 (5.01)	9.2	3.1	12.3
GRB-WB	$10^8 - 10^9$	0.00011 (0.00014)	0.000031 (0.000034)	0.0001 (0.00014)			
	$10^9 - 10^{10}$	– (–)	– (–)	– (–)			
	$10^{10} - 10^{11}$	– (–)	– (–)	– (–)	–		
	$10^{11} - 10^{12}$	– (–)	– (–)	– (–)	–		
	total	0.00013 (0.0002)	0.000034 (0.000038)	0.00016 (0.00024)	–	–	–
TD-SLBV	$10^8 - 10^9$	0.23 (0.29)	0.11 (0.13)	0.34 (0.42)			
	$10^9 - 10^{10}$	0.49 (0.64)	0.14 (0.17)	0.63 (0.81)			
	$10^{10} - 10^{11}$	0.38 (0.54)	0.07 (0.10)	0.45 (0.64)	–		
	$10^{11} - 10^{12}$	0.13 (0.22)	0.02 (0.02)	0.15 (0.24)			
	total	1.23 (1.69)	0.34 (0.42)	1.57 (2.11)	–	–	–
TD-SLSC	$10^8 - 10^9$	0.006 (0.007)	0.004 (0.004)	0.010 (0.011)			
	$10^9 - 10^{10}$	0.021 (0.028)	0.009 (0.011)	0.030 (0.039)			
	$10^{10} - 10^{11}$	0.035 (0.052)	0.010 (0.014)	0.045 (0.066)	–		
	$10^{11} - 10^{12}$	0.037 (0.060)	0.005 (0.008)	0.042 (0.068)			
	total	0.099 (0.147)	0.028 (0.037)	0.127 (0.184)	0.15	0.07	0.22
Z-burst	$10^8 - 10^9$	0.014 (0.017)	0.011 (0.012)	0.025 (0.029)			
	$10^9 - 10^{10}$	0.074 (0.099)	0.040 (0.049)	0.114 (0.148)			
	$10^{10} - 10^{11}$	0.188 (0.277)	0.067 (0.093)	0.255 (0.370)	–		
	$10^{11} - 10^{12}$	0.315 (0.519)	0.049 (0.078)	0.364 (0.597)			
	total	0.59 (0.91)	0.17 (0.23)	0.76 (1.14)	0.79	0.40	1.19

Table 5: Annual nominal event rates produced by Earth-skimming  $\nu_\tau$ 's for the fluorescence Telescope Array detector (10 stations) calculated according to (3.2) with  $D=0.1$  and the aperture for the detections of  $\tau$  leptons through their dominant decay to electromagnetic showers taken from [25]. The numbers in parentheses are the rates resulting from the largest Regge-inspired  $\nu N$  cross section in Fig.7. The estimated total TA rates of [26] are also displayed, where available. The total Auger rates are obtained from folding the effective Auger aperture [43] ('BS+PP+DIS low' curve in Fig.9 of [43]) with the appropriate cosmic  $\nu_\tau$ -fluxes in Fig.1. These latter event rates refer to the Auger ground array (not the fluorescence detector) with a duty cycle of 1.

flux	$E_\tau(\text{GeV})$	detectors		
		TA	TA([26])	Auger([43])
AGN-SS	$10^8 - 10^9$	1.07 (1.12)		
	$10^9 - 10^{10}$	0.0006 (0.0006)		
	$10^{10} - 10^{11}$	— (—)	—	—
	$10^{11} - 10^{12}$	— (—)		
	total	1.07 (1.12)	—	1.15
AGN-M95	$10^8 - 10^9$	47.4 (46.1)		
	$10^9 - 10^{10}$	14.8 (12.8)		
	$10^{10} - 10^{11}$	0.25 (0.19)	—	—
	$10^{11} - 10^{12}$	— (—)		
	total	62.5 (59.1)	42.8	72.8
GRB-WB	$10^8 - 10^9$	0.0035 (0.0036)		
	$10^9 - 10^{10}$	0.0002 (0.0002)		
	$10^{10} - 10^{11}$	— (—)	—	—
	$10^{11} - 10^{12}$	— (—)		
	total	0.0037 (0.0038)	—	0.0039
TD-SLBY	$10^8 - 10^9$	7.62 (7.22)		
	$10^9 - 10^{10}$	5.21 (4.35)		
	$10^{10} - 10^{11}$	0.54 (0.40)	—	—
	$10^{11} - 10^{12}$	0.008 (0.005)		
	total	13.4 (11.98)	—	17.0
TD-SLSC	$10^8 - 10^9$	0.19 (0.17)		
	$10^9 - 10^{10}$	0.23 (0.18)		
	$10^{10} - 10^{11}$	0.05 (0.04)	—	—
	$10^{11} - 10^{12}$	0.002 (0.001)		
	total	0.47 (0.39)	0.34	0.66
Z-burst	$10^8 - 10^9$	0.34 (0.29)		
	$10^9 - 10^{10}$	0.80 (0.63)		
	$10^{10} - 10^{11}$	0.27 (0.19)	—	—
	$10^{11} - 10^{12}$	0.017 (0.011)		
	total	1.43 (1.12)	1.19	2.18

Table 6: Contributions to the nominal TA event rates for given  $E_\tau$ -bins in Table 5 from various increasing  $E_\nu$ -bins of three representative cosmic neutrino fluxes.

flux		AGN-M95	TD-SLBY	Z-burst
$E_\tau$ [GeV]	$E_\nu$ [GeV]	TA	TA	TA
$10^8 - 10^9$	$10^8 - 10^9$	32.11	4.05	0.055
	$10^9 - 10^{10}$	15.04	3.27	0.19
	$10^{10} - 10^{11}$	0.26	0.28	0.082
	$10^{11} - 10^{12}$	—	0.012	0.017
total		47.4	7.6	0.34
$10^9 - 10^{10}$	$10^9 - 10^{10}$	13.59	3.87	0.35
	$10^{10} - 10^{11}$	1.17	1.28	0.37
	$10^{11} - 10^{12}$	0.0001	0.054	0.08
total		14.8	5.2	0.8
$10^{10} - 10^{11}$	$10^{10} - 10^{11}$	0.25	0.48	0.18
	$10^{11} - 10^{12}$	0.0002	0.062	0.09
total		0.25	0.54	0.27
$10^{11} - 10^{12}$	$10^{11} - 10^{12}$	—	0.008	0.017

Table 7: Total annual event rates for the Pierre Auger Observatory for horizontal air showers as implied by the SM and the additional contributions due to the exchange of KK gravitons in a low-scale scenario with large 'extra dimensions'. The rates are calculated according to (3.1), with the additional graviton KK exchange contribution given in (4.5), and using the geometrical acceptances of Fig.8. The first entry corresponds to using the unitarity interpolation (4.3) (dotted curve in Fig.10) and the second entry is the result of using (4.4) (dashed curve in Fig.10).

flux	$E_{sh}$ threshold $E_{th}/\text{GeV}$			
	$10^8$	$10^9$	$10^{10}$	$10^{11}$
AGN-SS	0.54/0.38	0.001/0.001	-/-	-/-
AGN-M95	401/880	151/398	7.2/27.9	0.001/0.007
GRB-WB	0.007/0.011	0.001/0.004	-/0.001	-/-
TD-SLBY	352/2996	267/2487	118/1350	19.8/289
TD-SLSC	47.0/703	42.4/624	27.5/407	7.3/114
Z-burst	342/6305	321/5696	233/3919	76.2/1250

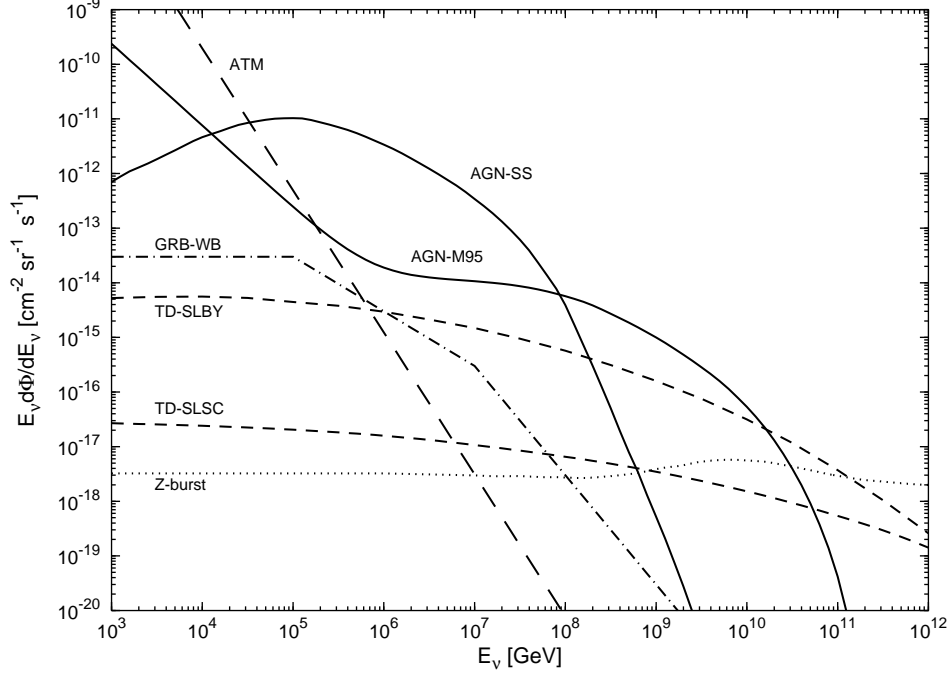


Figure 1: Representative differential fluxes of muon neutrinos ( $\nu_\mu + \bar{\nu}_\mu$ ) from active galactic nuclei (AGN-SS [9] and AGN-M95 [8]), gamma ray bursts (GRB-WB [11]), topological defects (TD-SLSC [14] and TD-SLBY [15]) and Z-bursts [18]. Due to naive channel counting in pion production and decay at the production site ( $\nu_e : \nu_\mu = 1 : 2$ ) and maximal mixing,  $\nu_e : \nu_\mu : \nu_\tau = 1 : 1 : 1$ , these fluxes are divided equally between  $\mu$ ,  $e$  and  $\tau$  neutrinos when they reach Earth (i.e. will be divided by a factor of 2). The background angle-averaged atmospheric (ATM) neutrino  $\nu_\mu + \bar{\nu}_\mu$  flux [19,20,21] is shown for illustration by the long-dashed curve.

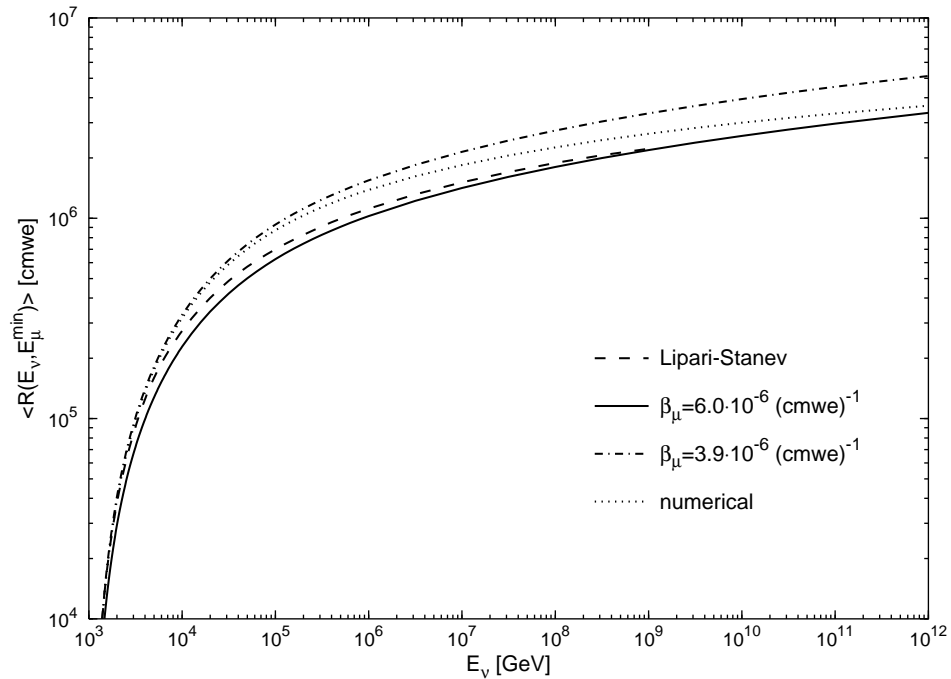


Figure 2: Mean ranges in rock of muons produced in CC interactions of neutrinos with energies  $E_\nu$  according to (2.5) with  $E_\mu^{min} = 1\text{TeV}$ . The analytic ranges follow from (2.7) for constant values of  $\alpha_\mu$  and  $\beta_\mu$ , and the numerical range follows from (2.6) using (2.8). The Lipari-Stanev range is taken from [48] which extends only up to  $10^9$  GeV.

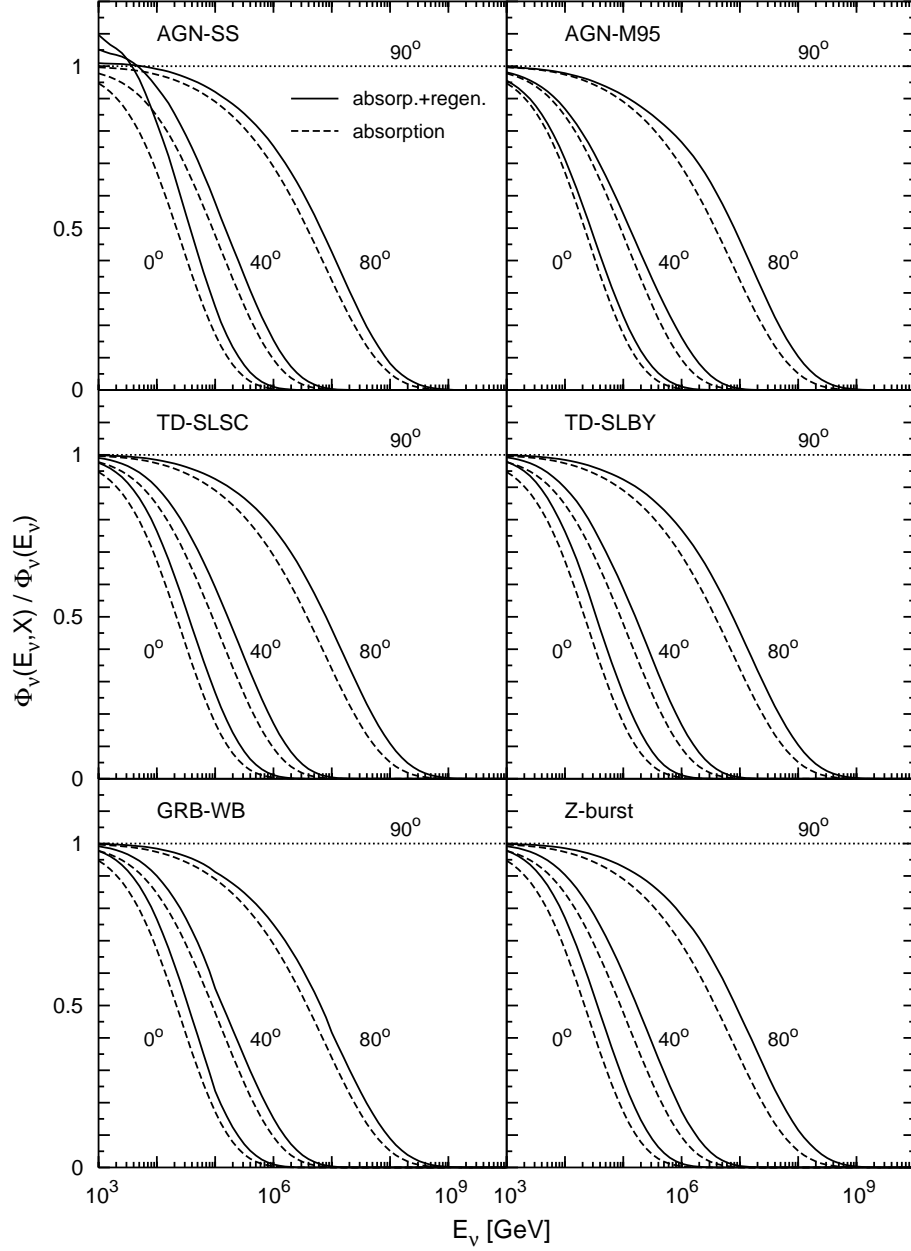


Figure 3(a): The differential shadow factor in (2.10) for three different nadir angles of cosmic neutrino fluxes incident at the Earth's surface with an initial flux  $\Phi_\nu(E_\nu, X = 0) \equiv \Phi_\nu(E_\nu) = \Phi(E_\nu)/4$  with the original total  $\nu_\mu + \bar{\nu}_\mu$  flux  $\Phi(E_\nu)$  being given in Fig.1. The dashed curves describe the attenuation just due to absorption where regeneration is omitted,  $\Psi \equiv 1$  in (2.10).

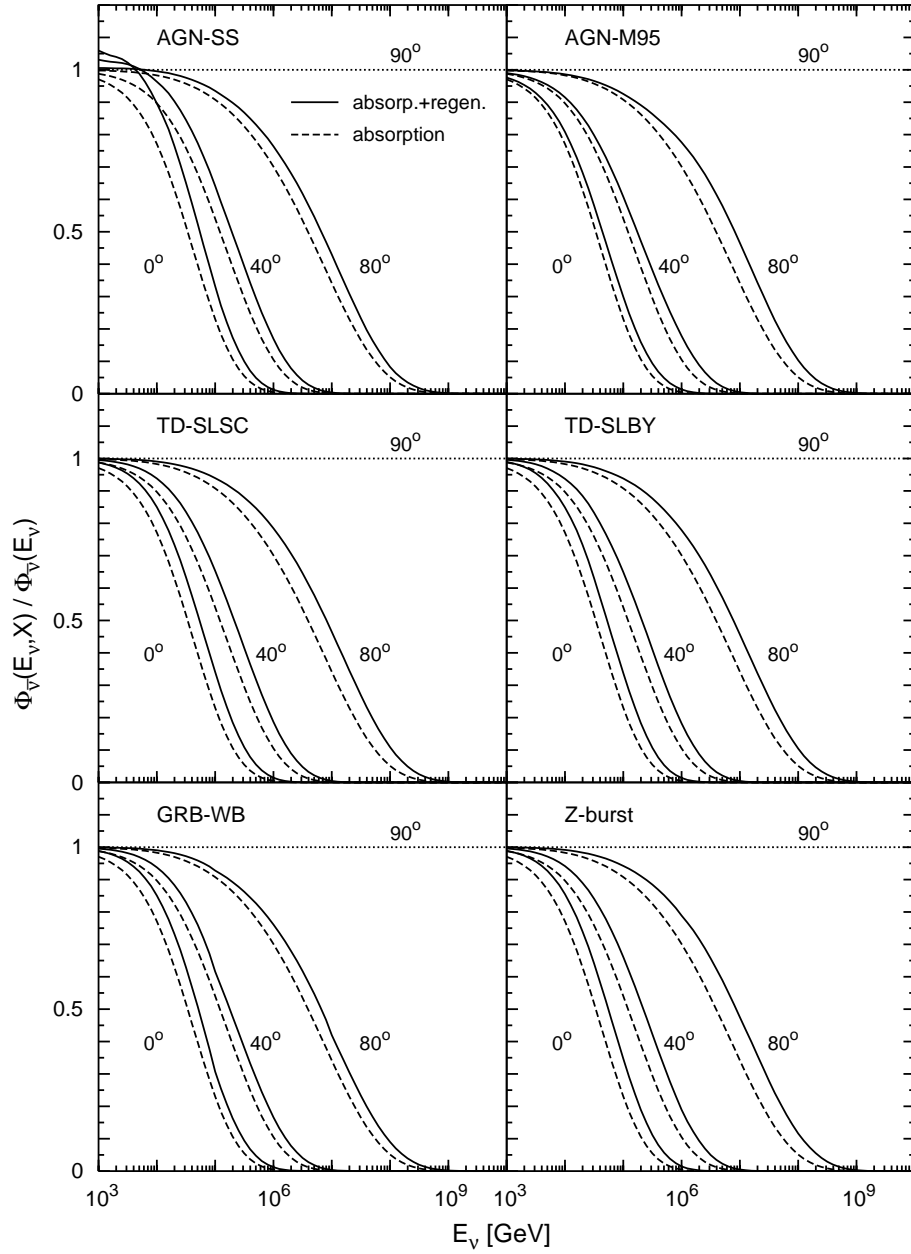


Figure 3(b): As in Fig. 3(a) but for antineutrinos where the initial flux at the Earth's surface is again given by  $\Phi_{\bar{\nu}}(E_{\nu}, X = 0) \equiv \Phi_{\bar{\nu}}(E_{\nu}) = \Phi(E_{\nu})/4$  with  $\Phi$  being given in Fig.1.

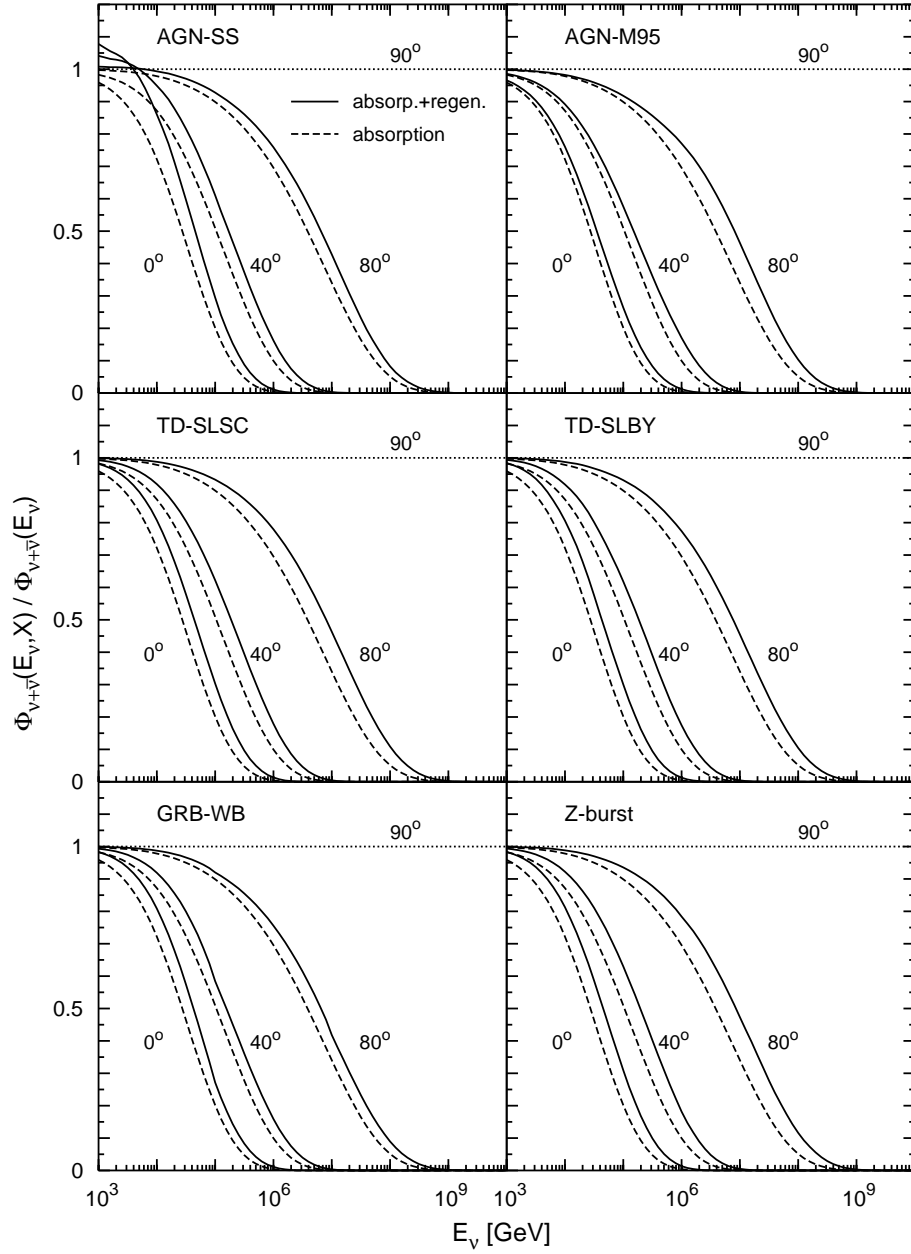


Figure 3(c): As in Fig. 3(a) but for the total neutrino plus antineutrino fluxes where the initial total flux at the Earth's surface is given by  $\Phi_{\nu+\bar{\nu}}(E_\nu, X = 0) \equiv \Phi_{\nu+\bar{\nu}}(E_\nu) = \Phi(E_\nu)/2$  with the original  $\Phi$  given in Fig.1.



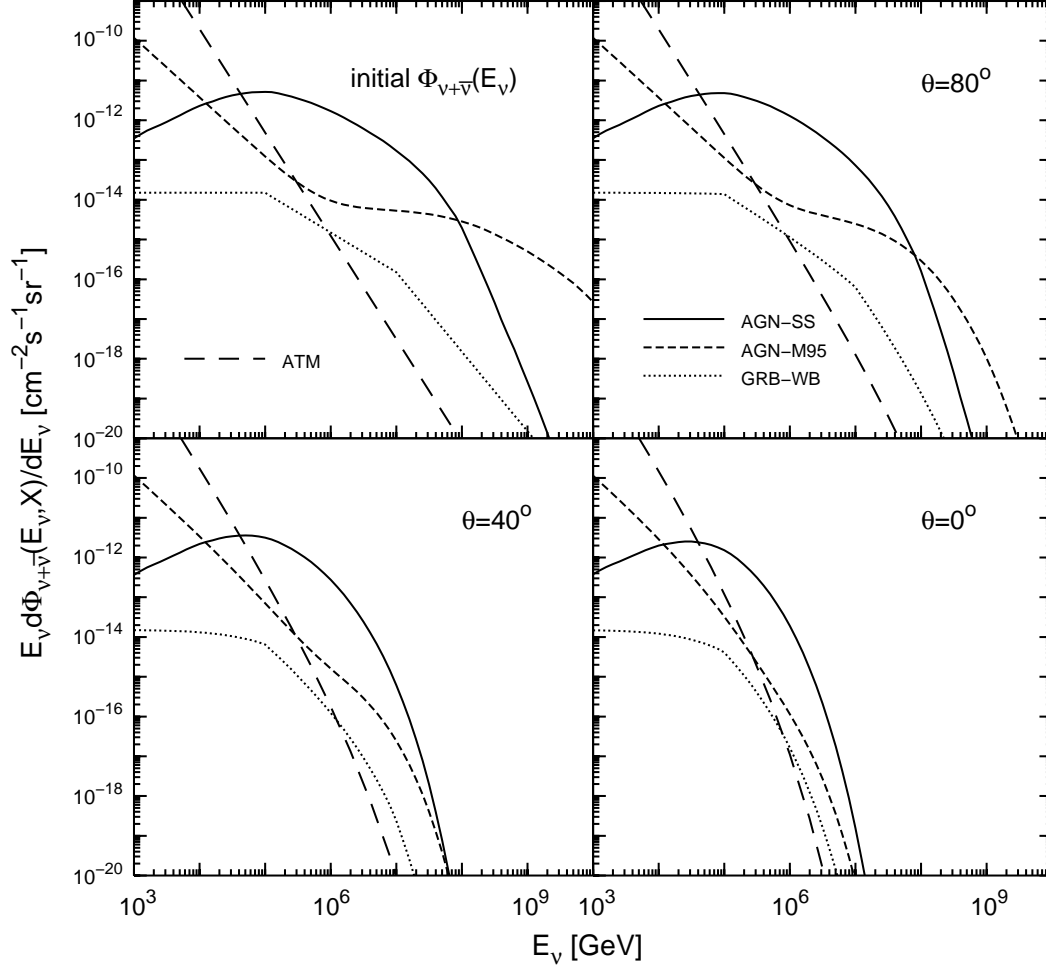


Figure 4(a): The initial  $\nu_\mu + \bar{\nu}_\mu$  flux at the Earth's surface  $\Phi_{\nu+\bar{\nu}}(E_\nu, X=0) \equiv \Phi_{\nu+\bar{\nu}}(E_\nu) = \Phi(E_\nu)/2$ , with  $\Phi(E_\nu)$  in Fig.1, and the flux at the detector  $\Phi_{\nu+\bar{\nu}}(E_\nu, X)$  for three different nadir angles corresponding to two models for AGN neutrinos, AGN-SS [9] and AGN-M95 [8], and to neutrinos from gamma ray bursts, GRB-WB [11]. The division by a factor of 2 of the original cosmic fluxes  $\Phi(E_\nu)$  in Fig.1 is due to maximal mixing. The background atmospheric (ATM) neutrino flux is also shown for comparison.

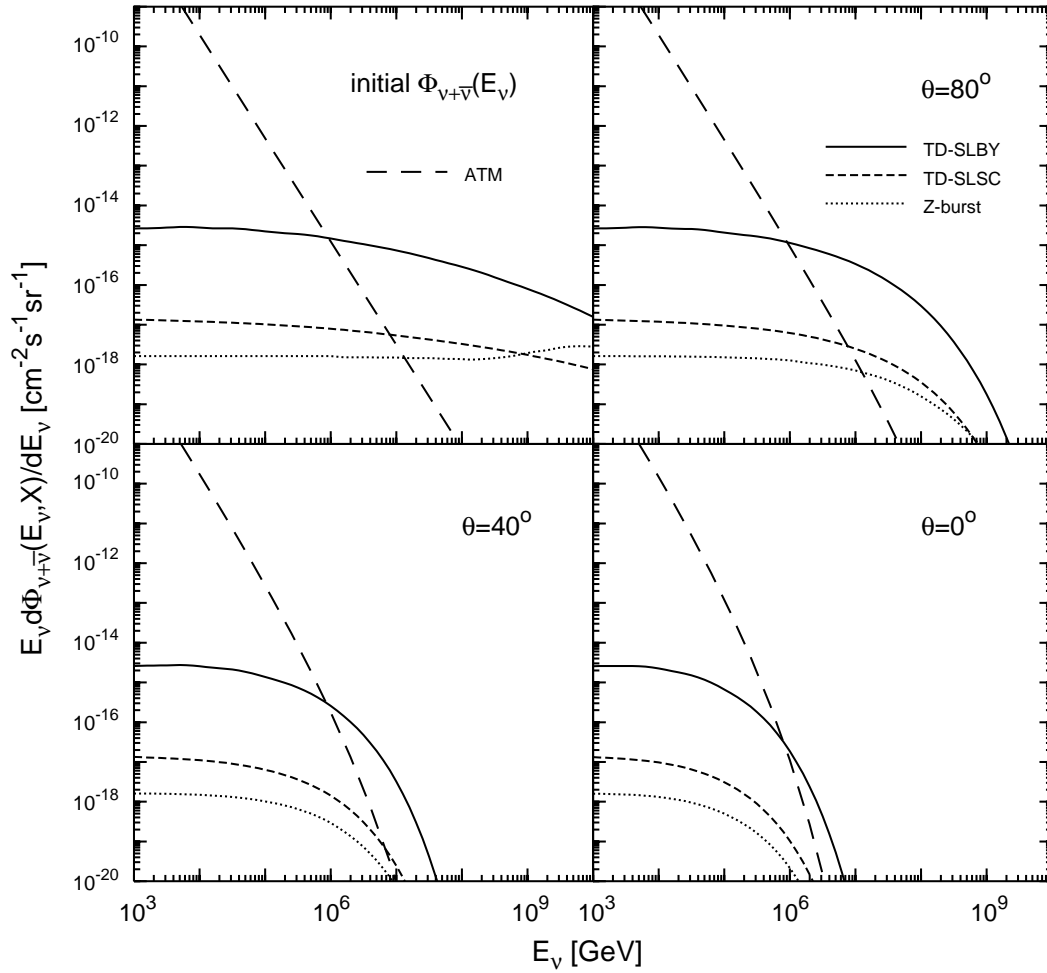


Figure 4(b): As in Fig.4(a), but showing neutrino fluxes from two topological defects models, TD-SLBY [15] and TD-SLSC [14], and from Z-bursts [18].

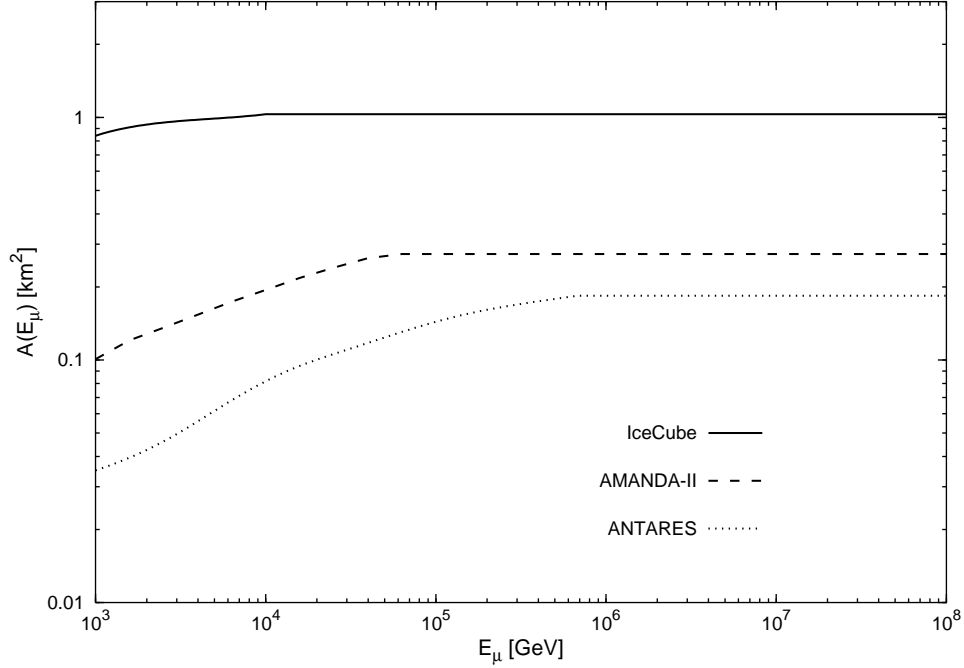


Figure 5: Effective energy dependent areas for the underground detectors ANTARES [39], Amanda-II [50] and IceCube [51] used for our calculations of total event rates.

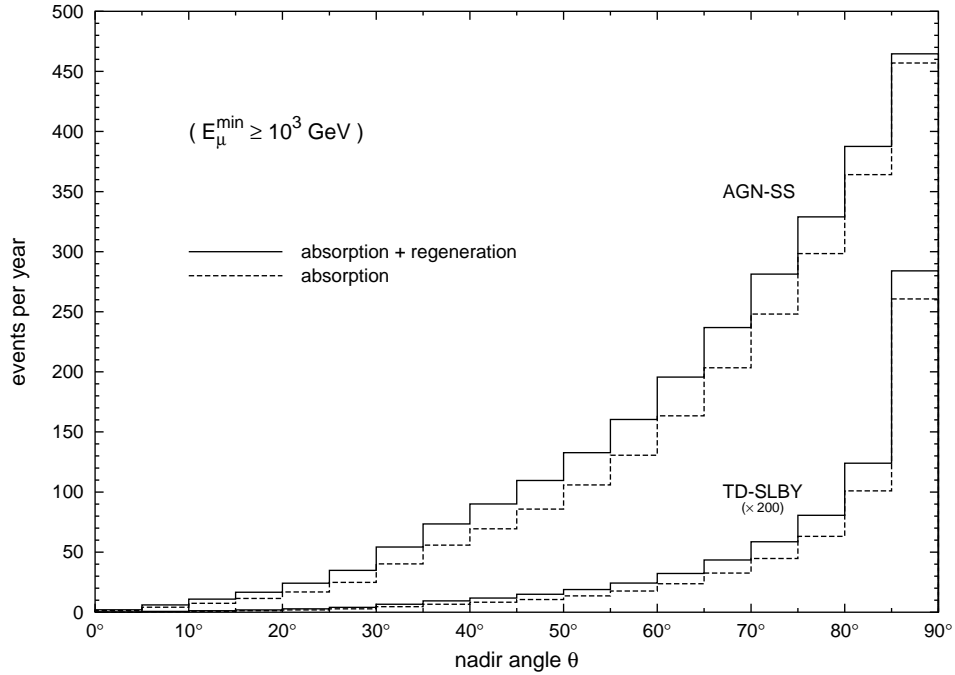


Figure 6: Nadir angular dependence of upward  $\mu^+ + \mu^-$  event rates per year for two representative neutrino flux models in Fig.1. The dashed histograms refer to events where the neutrino attenuation is caused just by absorption ( $\Psi \equiv 1$  in (2.12)) with no regeneration. For definiteness an effective energy-independent detector area of  $A_{eff} = 1 \text{ km}^2$  has been used in (2.1) (cf. Fig.5). The TD-SLBY rates have been multiplied by a factor of 200.

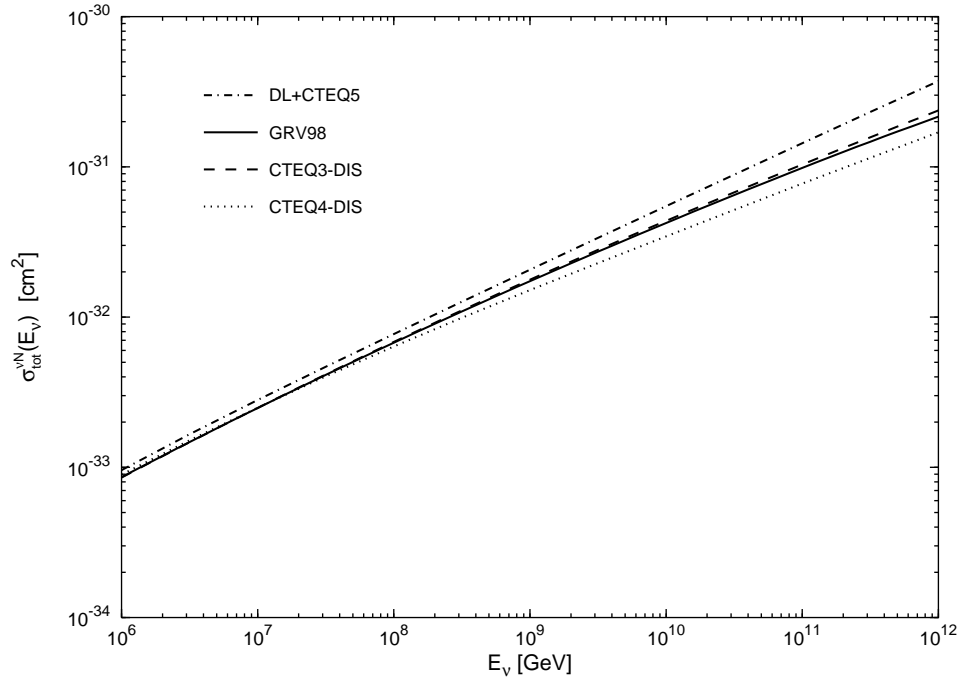


Figure 7: Total (CC+NC)  $\nu$ N cross sections. The dashed-dotted curve refers to the cross section calculated using the DL+CTEQ5 structure functions [62] with their Regge model inspired small-x extrapolation [61]. Our nominal results are based on GRV98 [32], or equivalently on the CTEQ3-DIS [37] parton distributions. For illustration the results based on CTEQ4-DIS [38] are shown as well.

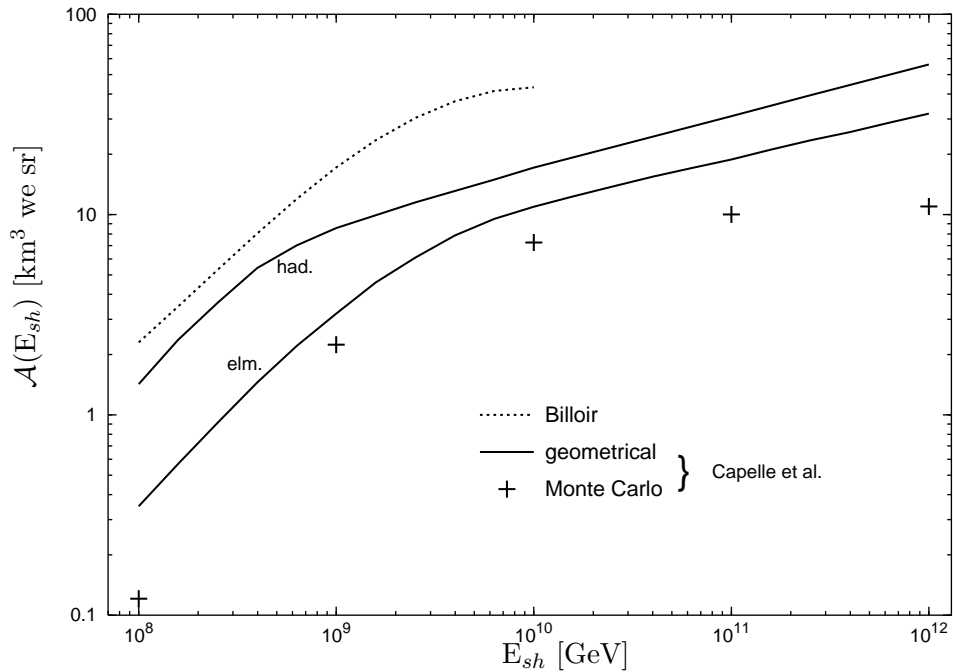


Figure 8: Acceptances versus shower energy needed for calculating near-horizontal air shower event rates according to (3.1) for the Auger detector. The solid curves correspond to a geometrical integration for electromagnetic and hadronic showers of Capelle et al. [28] and the crosses are the results of a Monte Carlo simulation of all showers [28] which can be considered as a lower bound of the acceptance. For comparison the acceptance for all showers as estimated by Billoir [65] is shown by the dotted curve.

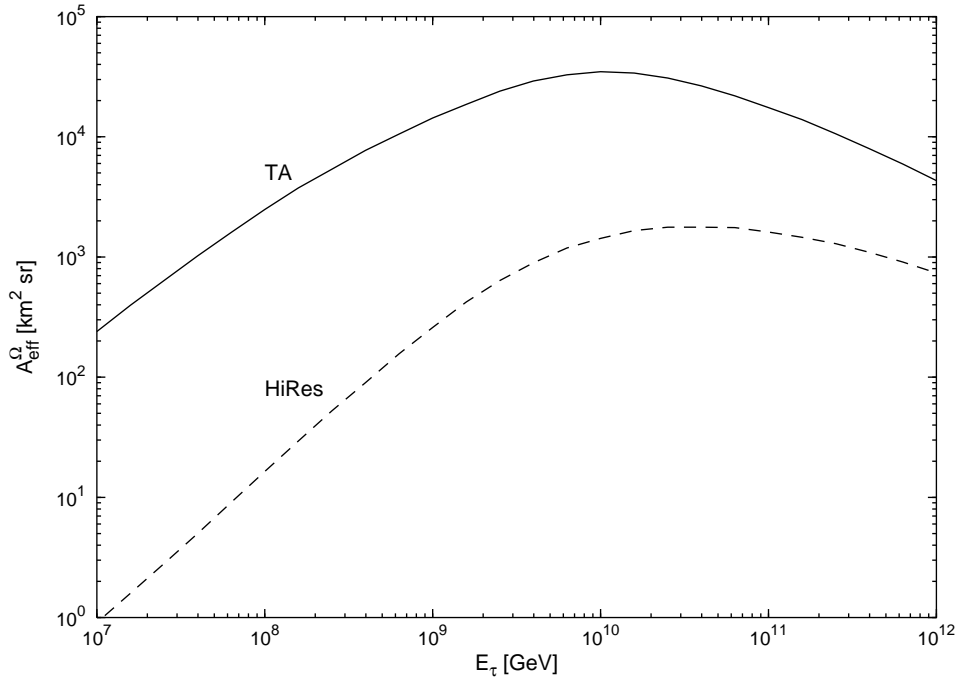


Figure 9: Effective (geometric) aperture estimates [25] for the detection of Earth-skimming  $\tau$  leptons through their most promising and dominant decays to electromagnetic showers for the Telescope Array (one station) and the HiRes detector. The TA aperture is expected to be somewhat smaller [67] due to effects such as the detector response, light propagation in air, and night sky background.

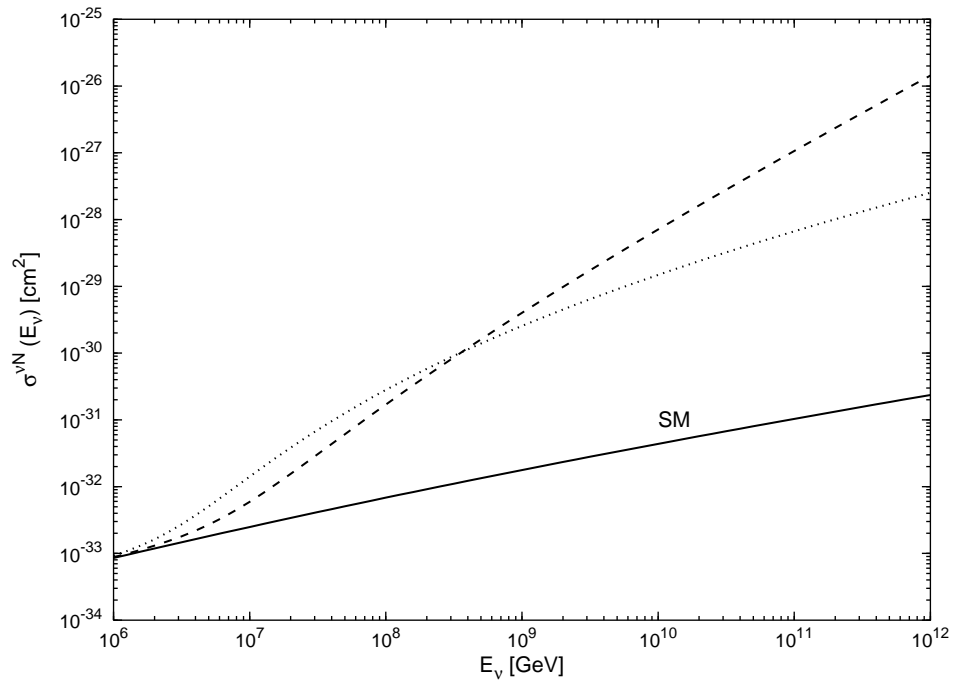


Figure 10: The nominal total  $\nu N$  cross section in the SM(CC+NC) compared to a scenario with large 'extra dimensions' using two different unitarity extrapolations between perturbative and nonperturbative regimes: the dotted line refers to Eq. (4.3) and the dashed one to Eq. (4.4).